IS LARGE-SCALE PRETRAINING THE SECRET TO GOOD DOMAIN GENERALIZATION?

Piotr Teterwak[*], **Kuniaki Saito**[*], **Theodoros Tsiligkaridis**[†], **Bryan A. Plummer**[*‡], **Kate Saenko**[*‡]
[*]Boston University [†]MIT Lincoln Laboratory,
{piotrt,kesaito,bplum,saenko}@bu.edu tsili@ll.mit.edu

ABSTRACT

Multi-Source Domain Generalization (DG) is the task of training on multiple source domains and achieving high classification performance on unseen target domains. Recent methods combine robust features from web-scale pretrained backbones with new features learned from source data, and this has dramatically improved benchmark results. However, it remains unclear if DG finetuning methods are becoming better over time, or if improved benchmark performance is simply an artifact of stronger pre-training. Prior studies have shown that perceptual similarity to pre-training data correlates with zero-shot performance, but we find the effect limited in the DG setting. Instead, we posit that having perceptually similar data in pretraining is not enough; and that it is how well these data were learned that determines performance. This leads us to introduce the Alignment Hypothesis, which states that the final DG performance will be high if and only if alignment of image and class label text embeddings is high. Our experiments confirm the Alignment Hypothesis is true, and we use it as an analysis tool of existing DG methods evaluated on DomainBed datasets by splitting evaluation data into In-pretraining (IP) and Out-of-pretraining (OOP). We show that all evaluated DG methods struggle on DomainBed-OOP, while recent methods excel on DomainBed-IP. Put together, our findings highlight the need for DG methods which can generalize beyond pretraining alignment. We release DomainBed-OOP at https://huggingface.co/datasets/PTeterwak/DomainBed_OOP.

1 INTRODUCTION

Domain Generalization (DG) addresses the challenge of enabling AI models to generalize from known domains to unseen ones, a critical task given the inevitable distribution shifts between training and real-world deployment (Saenko et al., 2010). DG pipelines typically consist of three stages: pretraining a model on a large, general dataset; finetuning the model with one or more source domains; and finally evaluating the model on target domains that are distinct from source domains. DG methods increasingly rely on huge-scale foundation models for initialization(*e.g.*, (Shu et al., 2023; Cha et al., 2022; Addepalli et al., 2024)). Simultaneously, finetuning has increasingly incorporated regularization to prevent catastrophic forgetting. As a result, it remains unclear whether DG methods are genuinely improving or if benchmark performance gains are simply due to stronger pre-training, possibly with the target domains within the hundred million-scale pre-training data (Mayilvahanan et al., 2025), combined with regularization.

In this work, we examine the reliance of recent state-of-the-art CLIP-based DG methods on pretrained features. While prior studies have shown that perceptual similarity to pre-training data explains zero-shot performance—referred to as the Image Similarity Hypothesis (Mayilvahanan et al., 2024)—we find this relationship to be limited in the DG setting. Despite evidence of target domains being present in pre-training (Figure 4), we find that perceptual similarity alone does not fully explain accuracy in the DG context (Section 3). We argue that it is not just the presence of similar data in pre-training that matters, but also how well this data was learned. To this end, we introduce the Alignment Hypothesis, which states that pre-trained alignment between image and class

[‡]Indicates equal contribution as senior author

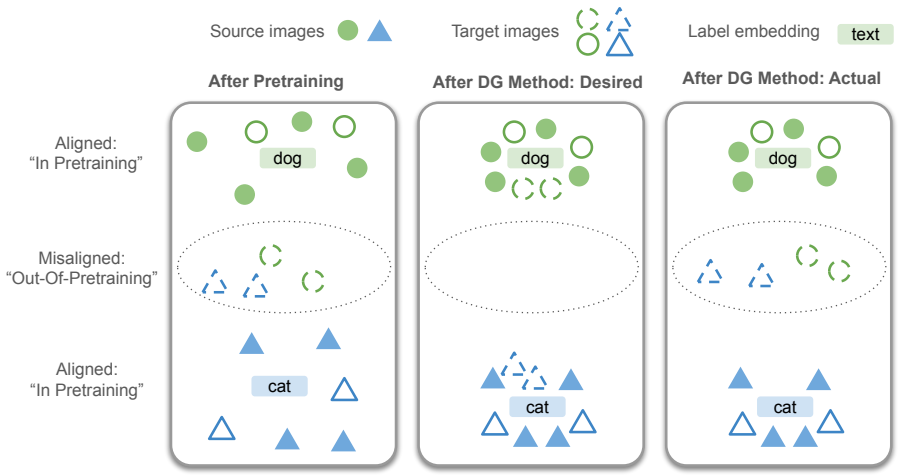

Figure 1: **An overview of desired and actual behaviour of DG methods. 1)** DG methods are initialized with foundation models like CLIP. Pre-trained embeddings are relatively well aligned with ground truth labels on both source and target data for most samples (In-Pretraining, IP), but some samples are not well aligned (Out-of-pretraining, OOP). **2)** An ideal DG method would strengthen alignment for both OOP and IP data with ground truth labels. **3)** Our analysis shows that DG methods only result in strong alignment for IP data, leaving OOP data misaligned (Figure 2).

embeddings is still predictive of DG performance even after source finetuning. We note that we do not make assumptions of how or why alignment arose. In the Alignment Hypothesis, pre-training alignmnent is used as a measure for how well a sample is learned. We find that performance for low alignment samples can be almost 0, while performance for high alignment samples is close to perfect. These results confirm the Alignment Hypothesis. As illustrated in Figure 1, these findings suggest that current DG methods largely fail to learn new, general features from the source data when the pretraining does not already provide a strong alignment.

The confirmation of the Alignment Hypothesis gives us a tool to separate aligned and well learned in-pretraining (IP) data from misaligned and poorly learned out-of-pretraining (OOP) data for a particular backbone, and we do so for five DG datasets with OpenCLIP-ViT/B-16. We call the resulting splits DomainBed-IP and DomainBed-OOP. Evaluating on DomainBed-IP/OOP offers a view of where current DG methods fail and where they succeed. We focus on CLIP-based methods, as they are used in state-of-the-art DG methods (Addepalli et al., 2024; Cho et al., 2023; Shu et al., 2023; Mao et al., 2024); we believe extensions to pure vision models such as DINOv2 (Oquab et al., 2023) represent interesting future work. We find that all methods, including those considered state-of-the-art, perform poorly on OOP data, *i.e.*, data that the pretrained backbone hadn't already aligned well. Furthermore, recent state-of-the-art methods do not outperform older methods on OOP data; CLIPood (Shu et al., 2023) slightly under performs a combination of older methods (MIRO (Cha et al., 2022) + MPA (Arpit et al., 2022)) on DomainBed-OOP. At the same time, existing DG methods show exceptional performance on DomainBed-IP, sometimes even outperforming an oracle model *trained on the target domain*. These results suggest that future research should aim to enhance DG methods on low-alignment data. In summary, we make the following contributions:

- **Introduce the Alignment Hypothesis**: We demonstrate that pre-training alignment between image and class text embeddings is a stronger predictor of Domain Generalization (DG) success than the previously proposed Image Similarity Hypothesis (Mayilvahanan et al., 2024). Based on this, we define In-Pretraining (IP) as data well-aligned with pre-trained embeddings, and Out-of-Pretraining (OOP) as data with weaker alignment.
- **Propose a new IP/OOP evaluation framework**: We demonstrate that splitting target data by its alignment with the pre-trained backbone can effectively test Out-of-Pretraining (OOP) generalization. We release IP/OOP splits for DomainBed datasets.
- **Expose strengths and limitations of state-of-the-art DG methods**: Using DomainBed-IP/OOP we find that leading DG methods perform well on data well-aligned by pre-training but struggle on misaligned samples, emphasizing the need for methods that move beyond reliance on pre-training.

2 RELATED WORK

Multi-Source Domain Generalization: Domain Generalization aims to mitigate the impacts of domain shifts between source (training) and target (deployment) domains. These can include subpopulation shifts where all testing subpopulations are present in the training data but in different proportions (Dehdashtian et al., 2024), or it could be the case we consider in this work where the testing subpopulation is not at all present in the training subpopulation. Although we focus on the multi-source domain generalization task, where domains between train and test are completely disjoint, our analysis can be extended to other types of generalization. One standard approach is **domain-invariant feature learning**, which leverages domain labels to learn domain-invariant features. CORAL (Sun & Saenko, 2016) aligns second-order statistics, while DANN (Ganin et al., 2016) and ADDA (Tzeng et al., 2017) uses an adversarial loss. Gulrajani & Lopez-Paz (2020) show that ERM, which does not align features between domains, can outperform most prior work while being easier to tune. Another common approach is **domain-aware data augmentation** to expand the training domain to become closer to or even overlap the target domain. Inter-domain mixup (Yan et al., 2020) blends images from different domains. Similarly, style transfer can diversify training images (Zhong et al., 2022). **Deep ensembles** are effective for domain generalization (Arpit et al., 2022). Since they are computationally inefficient for inference, many recent works average model weights from either multiple finetuning runs or from a single training trajectory (Cha et al., 2021; Arpit et al., 2022; Rame et al., 2022; Jain et al., 2023; Li et al., 2023; Shu et al., 2023). More recently, several methods perform **regularized finetuning** towards the initialization of a pretrained model. This works under the assumption that pretrained features are useful for target data, and should not be unlearned. The general idea can be applied to weight space (L2SP (Xuhong et al., 2018)), feature space (MIRO (Cha et al., 2022)), or output space (CAR-FT (Mao et al., 2024),CLIPood (Shu et al., 2023)).

Large-Scale Pretraining for DG: Recent DG literature (Cho et al., 2023; Cha et al., 2022; Addepalli et al., 2024; Mao et al., 2024; Arpit et al., 2022) leverages large-scale pretrained initializations stronger than ImageNet (Russakovsky et al., 2015), and CLIP (Radford et al., 2021) is the most common choice. CLIP leverages a cross-domain contrastive loss to align images and captions. Due to the large scale of training data (typically at least 400 million samples) and the free-form nature of the text, CLIP enables effective zero-shot classification and learns features that generalize very well. Other choices for very strong pretraining include SWAG (Singh et al., 2022) and DinoV2 (Oquab et al., 2023). SWAG uses supervision from Instagram hashtags, while DinoV2 is trained without text supervision and instead relies on augmentation-based alignment. While our analysis focuses on image-text models like CLIP due to its popularity, the concept of alignment can extend to other types of pretraining models. We leave the exploration of this extension to future work.

Impact of Data on Model Performance: Several recent studies have explored the influence of pretraining data on model performance. Mayilvahanan et al. (2024) investigated how the presence of perceptually similar images in CLIP (Radford et al., 2021) pretraining affects performance, introducing the Similarity Hypothesis, which posits that nearest neighbor similarity is strongly correlated with zero-shot accuracy. Mayilvahanan et al. (2025) show that domain contamination in the pretraining has substantial impact on DG performance. Udandarao et al. (2024) demonstrated that concept frequency in pretraining is correlated with zero-shot performance and introduced a dataset focusing on infrequent concepts. Fang et al. (2022) found that diversity in pretraining data is critical for improving performance on benchmarks such as ImageNetV2 (Recht et al., 2019), ImageNet-R (Hendrycks et al., 2021), ImageNet-Sketch (Wang et al., 2019), and ObjectNet (Barbu et al., 2019). However, these studies focus on the zero-shot setting, where models are evaluated without further training. In contrast, we examine the domain generalization setting, where pre-trained models are fine-tuned on source domains and tested on held-out target domains. Yu et al. (2024) recommend using self-supervised pre-training to avoid data label leakage. In contrast we study DG model behavior in the more realistic setting of CLIP-pretraining. Our findings suggest that comparing target images to pre-trained images, as proposed by Mayilvahanan et al. (2024), is less predictive of final DG performance than directly measuring the alignment between the image and its class embedding.

3 ANALYZING THE ROLE OF PRETRAINING IN DOMAIN GENERALIZATION

This work explores Multi-Source Domain Generalization for classification, where samples from multiple source domains (*e.g.*, sketches, product photos) and a held-out target domain (*e.g.*, wildlife

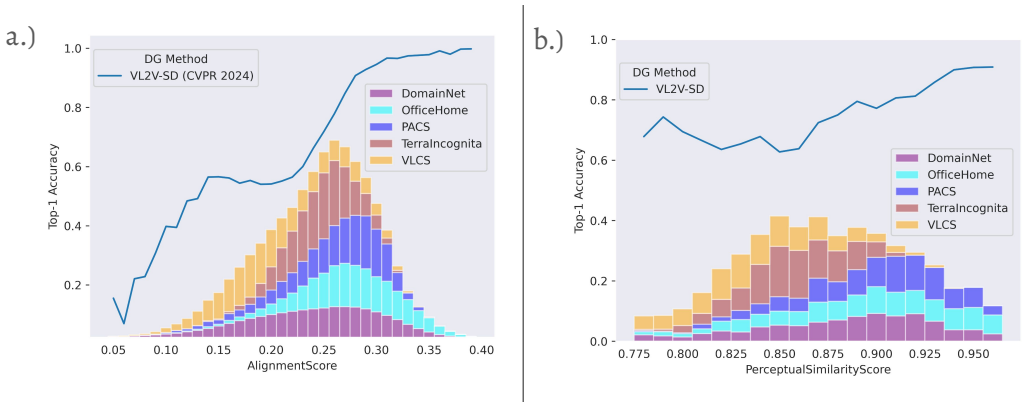

Figure 2: **Comparing the Predictive Power of the Alignment and Image Similarity Hypotheses for Domain Generalization (DG). a.) Alignment Hypothesis**: The cosine similarity between image and ground truth text-label embedding after pre-training (Alignment Score) is highly predictive of model accuracy after fine-tuning on five DG datasets, with Alignment Score distributions shown in the colored histograms. This suggests that image-text pairs well-aligned during pre-training result in better performance on target tasks. **b.) Image Similarity Hypothesis:** In contrast, the cosine similarity between a test image and its closest match from the pre-training set (Perceptual Similarity Score) shows weaker predictive power for accuracy, implying that visual resemblance alone is less indicative of downstream performance.

camera images) are annotated with both domain and class labels. We construct a training dataset by aggregating all sample-label pairs from all training domains $d \in \{d_1, \ldots, d_n\}$, denoted as

$$D = \{(X^{d_1}, Y^{d_1}), \ldots, (X^{d_n}, Y^{d_n})\}.$$

We initialize a classifier f with a contrastively pre-trained vision-language model (*e.g.*, CLIP) and finetune it on D. The scale of pre-training datasets is many orders of magnitude larger than that of source datasets. Most methods fully fine-tune f, though LP-FT (Kumar et al., 2021) fine-tunes the linear probe before the main network and Attention Tuning (Teterwak et al., 2023; Touvron et al., 2022) only tunes attention layers. The performance is then evaluated on a held-out testing domain d_{test}. The key assumption is that d_{test} has a different distribution from the source domains.

We aim to analyze how reliant existing DG methods are on pre-training. A recent analysis of CLIP proposed the Image Similarity Hypothesis (Mayilvahanan et al., 2024), which supposes that high CLIP performance on a given test sample is a result of highly similar nearest-neighbor images in pre-training, and tested it on zero-shot classification tasks. They found a strong correlation between nearest-neighbor similarity and zero-shot classification performance, but did not analyze OOD performance after fine-tuning. Therefore, we apply an equivalent testing setup for the DG setting, where a pre-trained model is fine-tuned on a source distribution and tested on a different target distribution. We find only a limited influence of image similarity in Section 3.1. To better understand the role of pretraining in domain generalization, we introduce the Alignment Hypothesis, which we explore in detail in Section 3.2. We later use the Alignment Hypothesis to split DG datasets and analyze existing DG methods (Section 4).

3.1 Testing the Image Similarity Hypothesis

The **Image Similarity Hypothesis** (Mayilvahanan et al., 2024) posits that test performance improves when there are perceptually similar images in the pre-training dataset. The PerceptualSimilarityScore measures perceptual similarity and is defined as the cosine similarity between a target image I and its nearest neighbor I_k in pre-training:

$$\text{PerceptualSimilarityScore}(I, I_k) = \frac{\langle f_I(I), f_I(I_k) \rangle}{\|f_I(I)\| \cdot \|f_I(I_k)\|} \qquad \text{(Eq. 1)}$$

where $\langle \cdot, \cdot \rangle$ denotes the dot product, and$\|\cdot\|$ denotes the Euclidean norm (magnitude). To evaluate the Image Similarity Hypothesis, we bin held-out target domain samples from five DomainBed datasets

Algorithm 1 Evaluating the Image Similarity Hypothesis

Require: Target domain samples D_{target}, trained DG model M, pre-trained image encoder f_I,
for each sample $I \in D_{\text{target}}$ **do**
    Retrieve nearest neighbor of I in LAION-400M using f_I features, assign to I_k
    Compute PerceptualSimilarityScore(I, I_k) using Equation Eq. 1,
    Record correctness of $M(I)$
end for
Bin samples based on PerceptualSimilarityScore
Compute DG accuracy within each bin
return Accuracy for each bin

based on their PerceptualSimilarityScore and compute the accuracy of a Domain Generalization (DG) method independently for each bin. This procedure is detailed in Algorithm 1 and visualized in Figure 2. The PerceptualSimilarityScore is computed using approximate nearest neighbors over the LAION-400M dataset (Schuhmann et al., 2021) with the CLIP-retrieval library (Beaumont, 2022).

We evaluate the recent, high-performing *VL2V-SD* (Addepalli et al., 2024) method. The results are shown in Figure 2 (b). While the Image Similarity Hypothesis is somewhat predictive of DG performance, its influence is not very strong. This suggests that perceptually similar pretraining data alone may not guarantee high DG performance; additional factors, such as how effectively the nearest neighbors were aligned with the target concept, may also be significant.

3.2 Introducing the Alignment Hypothesis

To find a stronger predictor of DG accuracy than perceptual similarity, we focus on how effectively pre-training captures the relationship between an image and its label. This leads us to propose the **Alignment Hypothesis**, which states that if an input image and its corresponding text label (*e.g.*, 'A photo of a {cls}') are well-aligned in the embedding space, final DG performance will be high. Crucially, alignment is measured before source fine-tuning while DG performance is measured after adaptation. This allows us to isolate the contribution of fine-tuning. Since models like CLIP optimize image-text pairs using a contrastive loss, cosine similarity between image and text embeddings is an alignment measure well coupled to their training objective. Therefore, we use it as our metric of pre-training generalization. More formally:

$$\text{AlignmentScore}(I, T) = \frac{\langle f_I(I), f_T(T) \rangle}{\|f_I(I)\| \cdot \|f_T(T)\|} \qquad \text{(Eq. 2)}$$

where $f_I(I)$ is the embedding of the image before finetuning on source, and $f_T(T)$ is the embedding of the text. Relative to directly using the contrastive loss value which also depends on negatives, PerceptualSimilarityScore has a scale which aligns across datasets (Appendix B.6).

We verify the Alignment Hypothesis similarly to the Image Similarity Hypothesis, by binning samples using the AlignmentScore and computing accuracy for each bin using VL2V-SD. We provide the same analysis for many more DG methods in the Appendix Figure 11. In Figure 2 a.), we can see that the Alignment Hypothesis explains DG performance after source finetuning, significantly more strongly than for the Image Similarity Hypothesis in Figure 2 b.) This finding suggests that source fine-tuning in DG, which aims to achieve high performance across all target samples, only succeeds on those with high initial alignment.

4 Re-thinking Domain Generalization Benchmarking using the Alignment Hypothesis

Knowing that the Alignment Hypothesis holds for contrastively trained image-text models (Section 3), we can now use it as a tool to probe the performance of DG methods across different levels of pre-training alignment. We apply this approach to five widely-used DomainBed (Gulrajani & Lopez-Paz, 2020) DG datasets: VLCS (Fang et al., 2013), PACS (Li et al., 2017), OfficeHome (Ganin et al., 2016), TerraIncognita (Beery et al., 2018), and DomainNet (Peng et al., 2019). This section discusses how we create new splits for existing DG datasets using AlignmentScore. We start by com-

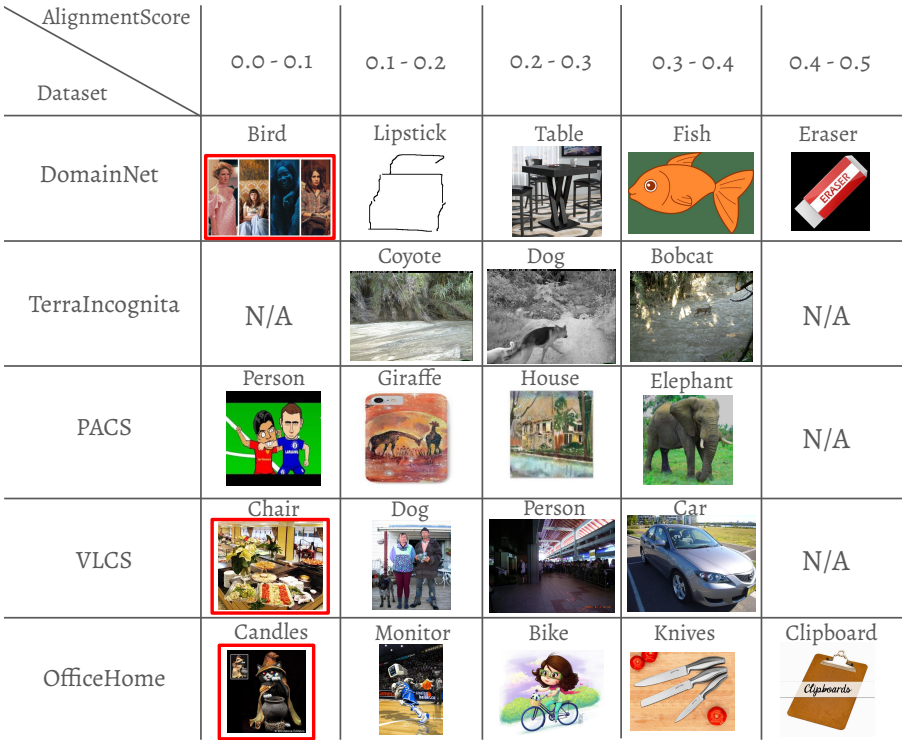

Figure 3: Representative DomainBed dataset samples and their labels at various AlignmentScore values. At very low AlignmentScores, most labels (red boxes) are incorrect. At very high AlignmentScores, text present in the image corresponds to the label.

puting AlignmentScore for all samples in 5 DG datasets (Figure 3). Based on our observation that some samples are mislabeled, we perform dataset cleaning (Section 4.1). Then we find an AlignmentScore threshold to split DG datasets into well aligned In-Pretraining (IP) and poorly aligned Out-of-Pretraining (OOP) evaluation subsets (Section 4.2), which we later use for evaluating DG methods (Section 5). In order to connect the AlignmentScore with the DG method, we use the same backbone both for splitting the datasets into IP and OOP subsets and for training DG methods.

4.1 Data Exploration and Cleaning

We start by visualizing the data of all the datasets at various AlignmentScore values. We show some representative samples in Figure 3. At very low scores, we find that a large fraction of labels are incorrect (red boxes in Figure 3). Thus, we divide the data into AlignmentScore intervals (*e.g.*, 0.00-0.05, 0.05-0.10, and so on, up to 0.2) and randomly sample 100 instances from each interval for every dataset. This allows us to systematically analyze the relationship between AlignmentScore and label accuracy across different score ranges. For each interval, we then count the fraction of mislabelled samples to better understand how low AlignmentScores are associated with labeling errors. We find that below an AlignmentScore of 0.15, label noise is unacceptably high, with all datasets suffering the most from mislabelling (Table 7 in Appendix). Therefore, we discard all samples with AlignmentScore less than 0.15 in DomainBed-IP/OOP. As shown in Table 8 (in the Appendix), we observe that the percentage of discarded samples due to mislabeling varies across datasets, with VLCS and DomainNet having the highest rates at 12.41% and 7.64%, respectively.

Furthermore, on the right side of Figure 3, we observe that at very high AlignmentScores (greater than 0.4), images often contain text directly related to the label. However, our goal is to evaluate visual recognition rather than text recognition (OCR), and CLIP is known to have strong OCR abilities (Fort, 2021), so we exclude all samples above AlignmentScore of 0.4 from DomainBed-IP/OOP. As shown in Table 8 (in the Appendix), only a small portion of data is removed due to OCR filtering (0.00-0.15% across datasets), but this issue may become more significant in future studies.

4.2 DATA SPLITTING

After filtering, we focus on determining a threshold to split the dataset into In-Pretraining (IP) and Out-of-Pretraining (OOP) subsets. We select 0.21 as the threshold, based on the trends observed in Figure 2 (a.)), as this is the point where performance begins to improve significantly, indicating that existing methods become more effective. While this threshold represents a somewhat subjective choice informed by observed patterns, we provide AlignmentScores in the released data, allowing researchers the flexibility to experiment with their own thresholds.

Figure 18 in the Appendix shows how this split impacts the size and composition of each dataset. For example, clipart in DomainNet is predominantly categorized as IP, likely due to its frequent presence on the internet and, therefore, web-scraped pre-training data. In comparison, TerraIncognita-OOP is more balanced domains, but exhibits substantial class shift between IP and OOP splits (Figure 17 in the Appendix), meaning some classes are better aligned than others during pre-training.

We further investigate the distinctions between the IP and OOP subsets using VisDiff (Dunlap et al., 2024), an LLM-based system that identifies differences between sets of images. For each combination of dataset, domain, and class—except for DomainNet, where we subsample roughly 15% of the combinations due to computational constraints—we independently sample up to 30 images from both the IP and OOP subsets. VisDiff employs CLIP (Radford et al., 2021) to compute an AUC-ROC score for the natural language differences proposed by the LLM, and we retain only those differences with an AUC score of 0.7 or higher. Results are presented in Appendix Table 9.

Several clear patterns emerge from our analysis. Contextual or environmental elements often overshadow the primary object indicated by the text label. For example, in the VLCS dataset's SUN09 domain, the OOP subset for the car class frequently features images described as "historical architecture," while in the Office Home dataset, real-domain bed images are deemed OOP if they include "child-themed decor." These findings imply that object size may also play a role. In the car example, visible architecture implies that the car occupies only a small portion of the image, and in the bed example, the presence of child-themed decor indicates that the entire bedroom is visible rather than just the bed. To test this hypothesis, we computed the object size of the ground truth labeled objects using bounding boxes generated by the open-world object detector OWLv2 (Minderer et al., 2023). Overall, object size is correlated with the AlignmentScore (see Appendix Figure 10), with the sole exception being the TerraIncognita dataset. This indicates that even the presence of small wildlife can substantially increase the AlignmentScore, and that the background vegetation does not present a significantly conflicting signal that is sometimes present in other datasets. Overall, our findings suggest that pre-training which better represents scenes with multiple objects or concepts may improve benchmark performance.

5 EXPERIMENTS

We aim to evaluate how well Domain Generalization (DG) methods perform across both pretraining-aligned (IP) and pretraining-misaligned (OOP) data. We adhere to the DomainBed evaluation methodology, where one domain is chosen as the target, and the remaining domains act as source domains. To maintain a sufficient amount of training data, we train all DG methods on the original, unsplit datasets. We use hyper-parameter values recommended by the original implementation authors for each method.

After training, models are evaluated separately on IP and OOP subsets, as well as the original, unsplit test domain. This allows us to measure how well each method generalizes to both pretraining-aligned and pretraining-misaligned data. We follow the literature's standard practice of computing performance per target domain and averaging the results across all domains. This method ensures that any domain imbalances do not disproportionately influence the final performance metrics.

5.1 ALGORITHMS

Explicit Regularization towards Pretraining: Several recent DG methods leverage explicit regularization towards the initialization. These methods generally operate either in weight space (by regularizing or freezing model parameters) or in feature space (by aligning internal feature representations with those of the pretrained model). *MIRO* (Cha et al., 2022) minimizes the Mutual

Information between DG model intermediate features and CLIP intermediate features. *Attention Tuning* (Teterwak et al., 2023; Touvron et al., 2022) freezes all parameters except those in the Multiheaded-Attention Layers. *VL2V-SD* (Addepalli et al., 2024) self-distills a linear combination of CLIP vision and text outputs into a model. *CLIPood* (Shu et al., 2023) regularizes both weights and output features. Weights are averaged between the pre-trained CLIP model and the fine-tuned model, and outputs are regularized using a loss that incorporates information from the pre-trained text encoder. *Linear Probe - Fine Tuning (LP-FT)* (Kumar et al., 2021) freezes the backbone, trains a linear probe, and then performs full finetuning. An untrained linear probe can cause finetuning to update the frozen backbone needlessly, potentially unlearning discriminative features. This biases the model towards pre-trained weights with smaller gradient updates. **Domain Invariance**: A classic idea for Domain Generalization is Domain Invariance in the feature space, where the model learns only class-discriminative features shared among all training/source domains. *CORAL* (Sun & Saenko, 2016) matches the second moments of features across different domains and has been shown to be highly effective (Gulrajani & Lopez-Paz, 2020). **Flat Optima**: Studies by Izmailov et al. (2018) and Cha et al. (2021) have shown that flat minima generalize better than sharp minima, as they make loss values less sensitive to perturbations in the loss surface, resulting in smaller increases in loss during domain shifts. *SWAD* (Cha et al., 2021) Averages model parameters during training, determining the interval over which to average using validation loss over source domain. *Model Parameter Averaging (MPA)* (Arpit et al., 2022) Starts averaging model parameters after a number of burn-in steps to find flat minima. *SAGM* (Wang et al., 2023) is an optimizer that explicitly optimizes for flat minima. **Baseline and Oracle**: We also train a baseline and oracle model for lower-bound and upper-bound reference. The baseline model is an Empirical Risk Minimization (ERM) model that is finetuned on source domains and evaluated on target domains, and has been found to be effective for the DG task (Gulrajani & Lopez-Paz, 2020). The oracle model is trained on an 80% training split of all domains and evaluated on a 20% test split. The oracle model removes the OOD aspect of generalization and provides a reasonable upper bound for DG methods. Finally, we add a zero-shot LAION-400M (Schuhmann et al., 2021) pre-trained ViT-B/16 from OpenClip, which is the pre-trained model used in our analysis.

5.2 Results

Table 1 reports results for the poorly pre-training aligned DomainBed-OOP, higly pre-training aligned DomainBed-IP, and standard DomainBed datasets. Underlined results highlight the best performance of any single method (excluding method combinations), while the bold numbers show the highest performance overall, excluding the upper bound and zeros-hot baseline. Overall, we find that AlignmentScore is highly predictive of performance. More detailed observations about the results follow, while a comparison to PerceptualSimilarityScore can be found in Appendix B.5.

DG methods perform well on DomainBed-IP: In most datasets within DomainBed-IP, domain generalization approaches achieve excellent performance. *On three out of five datasets (DomainNet, OfficeHome, and PACS), the best DG method even outperforms the oracle.* A notable exception is TerraIncognita, where CLIPood scores only 63.5%, far below the oracle's 93.4%, highlighting this dataset as a challenging outlier. Interestingly, all three datasets where performance exceeds the oracle have an average IP AlignmentScore of 0.28, while the others have a lower average AlignmentScore of around 0.26. Therefore, the underperformance of TerraIncognita may be partially explained by its lower IP AlignmentScore, suggesting that alignment plays a significant role in DG performance, even within the IP case. Another interesting observation is that on the IP subset, the zero-shot model can achieve performances greater than the finetuned models (for PACS and VLCS). *This means that, for IP-data, DG finetuning sometimes causes more catastrophic forgetting than learning of new features* We show additional analysis of zero-shot models in Appendix B.9.

DG Methods leave much to be desired on DomainBed-OOP, but are still stronger than ERM: In DomainBed-OOP, we observe that even the top-performing DG methods struggle with low-alignment data. For example, CLIPood achieves 57.1% accuracy, which is a significant drop compared to its performance on DomainBed-IP (84.7%) and DomainBed-All (78.1%). Despite this, DG methods still outperform Empirical Risk Minimization (ERM), which scores only 47.0% on DomainBed-OOP. Therefore DG methods are better equipped to handle domain shifts than ERM, possibly due to weak transfer of knowlegdge from pre-trained features. Nevertheless, there is still substantial room for improvement on low-alignment samples.

Table 1: Benchmarking DG methods on DB-IP/OOP. Domain generalization methods excel on high-alignment (IP) datasets—often even surpassing the oracle—while their performance noticeably drops on low-alignment (OOP) data, though still outperforming ERM.

DomainBed-IP	DomainNet	OfficeHome	PACS	TI	VLCS	Average
OpenCLIP ZS	74.9	88.9	98.5	36.8	95.9	79.0
CORAL (Sun & Saenko, 2016)	63.3	76.1	84.3	42.9	86.5	70.6
SAGM (Wang et al., 2023)	64.3	79.5	90.1	44.0	88.0	73.2
ERM* (Gulrajani & Lopez-Paz, 2020)	63.1	78.1	87.1	42.0	85.3	71.1
LP-FT (Kumar et al., 2021)	64.4	78.5	90.3	40.9	86.0	72.0
SWAD (Cha et al., 2021)	72.3	84.8	94.6	52.7	88.5	78.6
MIRO (Cha et al., 2022)	72.4	88.8	97.6	58.9	91.0	81.7
VL2V-SD (Addepalli et al., 2024)	78.1	**91.4**	98.0	48.1	92.4	81.6
Attn Tune (Teterwak et al., 2023)	69.2	84.8	96.4	53.0	88.7	78.4
MPA (Arpit et al., 2022)	73.6	85.1	95.4	54.4	90.7	79.8
CLIPOOD (Shu et al., 2023)	**78.9**	90.9	97.7	**63.5**	**92.5**	**84.7**
MIRO + SWAD	77.0	90.5	97.6	62.1	91.1	83.6
MIRO + MPA	78.2	90.7	**98.1**	62.6	91.0	84.1
Upper Bound (Target Finetune)	81.6	88.5	97.8	93.4	93.8	91.0

(a) Samples with high AlignmentScore values, indicating good pretraining alignment.

DomainBed-OOP	DomainNet	OfficeHome	PACS	TI	VLCS	Average
OpenCLIP ZS	26.3	48.1	81.4	4.5	80.2	48.1
CORAL (Sun & Saenko, 2016)	22.3	42.6	74.1	16.0	74.0	45.8
SAGM (Wang et al., 2023)	23.0	44.5	74.2	19.3	73.3	46.9
ERM* (Gulrajani & Lopez-Paz, 2020)	22.3	42.9	76.9	16.5	76.4	47.0
LP-FT (Kumar et al., 2021)	22.7	43.4	78.6	23.1	70.7	47.7
SWAD (Cha et al., 2021)	28.6	49.9	79.1	21.0	77.0	51.1
MIRO (Cha et al., 2022)	28.4	56.6	84.7	18.5	73.7	52.4
VL2V-SD (Addepalli et al., 2024)	31.8	56.6	85.0	15.9	79.1	53.7
Attn Tune (Teterwak et al., 2023)	26.8	51.4	84.2	20.3	76.1	51.8
MPA (Arpit et al., 2022)	29.6	51.0	82.7	22.2	79.5	53.0
CLIPOOD (Shu et al., 2023)	**33.9**	**63.9**	87.2	19.9	**80.7**	57.1
MIRO + SWAD	32.0	59.0	85.4	21.1	78.9	55.3
MIRO + MPA	33.1	60.0	**87.8**	**24.9**	80.3	**57.2**
Upper Bound (Target Finetune)	48.8	61.9	92.9	83.2	92.4	75.8

(b) Samples with lower AlignmentScore values, representing cases where pretraining alignment is weak.

DomainBed-All	DomainNet	OfficeHome	PACS	TI	VLCS	Average
OpenCLIP ZS	59.5	85.4	97.0	33.2	82.4	71.5
CORAL (Sun & Saenko, 2016)	50.6	73.2	83.2	39.6	78.5	65.0
SAGM (Wang et al., 2019)	51.5	76.4	87.5	41.0	80.4	67.3
ERM* (Gulrajani & Lopez-Paz, 2020)	50.5	75.0	85.2	39.0	77.9	65.5
LP-FT (Kumar et al., 2021)	51.3	75.5	88.4	38.5	78.0	66.3
SWAD (Cha et al., 2021)	57.9	81.8	92.4	49.0	80.1	72.2
MIRO (Cha et al., 2022)	57.5	85.8	96.4	54.3	81.1	75.0
VL2V-SD (Addepalli et al., 2024)	62.0	**88.3**	96.9	44.4	82.7	74.9
Attn Tune (Teterwak et al., 2023)	55.4	81.9	95.4	49.1	81.8	72.7
MPA (Arpit et al., 2022)	58.9	82.0	94.3	50.7	82.3	73.6
CLIPOOD (Shu et al., 2023)	**63.6**	**88.3**	96.8	**58.5**	**83.4**	**78.1**
MIRO + SWAD	61.4	87.6	96.6	57.4	82.0	77.0
MIRO + MPA	62.4	87.9	**97.2**	58.2	82.8	77.7
Upper Bound (Target Finetune)	70.4	86.2	97.2	92.4	87.9	86.8

(c) Performance of DG methods on unsplit DomainBed

SOTA methods do not consistently outperform older methods on OOP data: While CLIPood (Shu et al., 2023) clearly outperforms other methods on DomainBed-All with 78.1% accuracy, it performs comparably to older methods on DomainBed-OOP. For instance, MIRO + MPA (Cha et al., 2022; Arpit et al., 2022) achieves 57.2% on DomainBed-OOP, which is nearly the same as CLIPood's 57.1%. This suggests that CLIPood's primary advantage comes from well-aligned samples in DomainBed-IP, where it reaches 84.7% accuracy, half a percent better than the next-best method.

Model Parameter Averaging (MPA) boosts performance on OOP data: MPA performs significantly better than ERM on DomainBed-OOP, achieving 53.0% compared to ERM's 47.0%. This is half a percent better than MIRO on OOP data, despite being 2% worse than MIRO on IP data. When combined with MIRO, MPA delivers the best performance on DomainBed-OOP, scoring 57.2%, slightly surpassing CLIPood. This suggests that MPA can complement other regularization-based methods like MIRO. On DomainBed-IP, MIRO + MPA scores 84.1%, close to CLIPood's 84.7%, demonstrating versatility across both high- and low-alignment data. Interestingly, SWAD underperforms MPA on DomainBed-OOP by 2%, despite being conceptually similar. We attribute this to selecting the averaging interval on the source data, which introduces overfitting to source domains.

5.3 Discussion

As an increasing number of works in the Domain Generalization sub-field leverage pre-trained CLIP models for Domain Generalization benchmarks, it is important to better characterize the impacts of pre-training on DG. We leave the reader with the following takeaways:

Pre-training Alignment Predicts DG Performance: Our study demonstrates that pre-training alignment, measured as the cosine similarity between image and text embeddings, is a robust predictor of DG performance. This holds true even after source fine-tuning, highlighting that the quality of alignment achieved during pre-training has a significant impact on the generalization capability.

Current DG Methods Exploit Pre-training Rather Than Learning New Features: Our findings reveal a large difference in the performance of DG methods between pretraining-aligned (IP) and pretraining-misaligned (OOP) data. While state-of-the-art methods achieve near-oracle performance on IP data, they struggle significantly on OOP data. This indicates that current methods primarily leverage on pre-trained features rather than learning new, generalizable features from source data. Consequently, their success is heavily tied to the quality of pre-training, rather than fine-tuning.

Benchmarks Should Reflect Pre-training Reliance: The reliance on pre-trained alignment calls for a reevaluation of DG benchmarks. Existing benchmarks often aggregate results across all target data, masking the limitations of DG methods on low-alignment samples. To address this, we propose splitting evaluation datasets into In-Pretraining (IP) and Out-of-Pretraining (OOP) subsets. This provides a clearer picture of where DG methods succeed and where they fail. We hope that our proposed DomainBed-IP/OOP splits will guide the development of future methods that are better equipped to handle low-alignment data while maintaining performance on high-alignment samples.

6 Conclusion

We systematically explore how Domain Generalization (DG) methods rely on pre-trained feature alignment from models like CLIP. We hypothesize that the alignment between image and text embeddings during pre-training strongly predicts DG performance. Our experiments confirm this, showing that methods perform well on high-alignment samples (DomainBed-IP) but struggle on low-alignment data (DomainBed-OOP). Notably, state-of-the-art methods like CLIPood perform near oracle-level on aligned data but see significant drops on misaligned samples. This suggests current DG methods rely on pre-trained features and fail to learn new, generalizable features from source domains. Moving forward, two paths emerge: developing DG methods that better learn generalizable features, or focusing on improving pre-trained backbones. While foundation models will continue to advance, there will always be specialized distributions where they fail. Therefore we take the stance that improved DG finetuning remains an important avenure of research. We hope these findings inspire further research into improving generalization on low-alignment data, pushing DG beyond reliance on pre-trained alignment.

7 ACKNOWLEDGMENTS

DISTRIBUTION STATEMENT A. Approved for public release. Distribution is unlimited. This material is based upon work supported by the Under Secretary of Defense for Research and Engineering under Air Force Contract No. FA8702-15-D-0001. Any opinions, findings, conclusions or recommendations expressed in this material are those of the author(s) and do not necessarily reflect the views of the Under Secretary of Defense for Research and Engineering.

REFERENCES

Sravanti Addepalli, Ashish Ramayee Asokan, Lakshay Sharma, and R Venkatesh Babu. Leveraging vision-language models for improving domain generalization in image classification. *CVPR*, 2024.

Devansh Arpit, Huan Wang, Yingbo Zhou, and Caiming Xiong. Ensemble of averages: Improving model selection and boosting performance in domain generalization. *Advances in Neural Information Processing Systems*, 35:8265–8277, 2022.

Andrei Barbu, David Mayo, Julian Alverio, William Luo, Christopher Wang, Dan Gutfreund, Josh Tenenbaum, and Boris Katz. Objectnet: A large-scale bias-controlled dataset for pushing the limits of object recognition models. *Advances in neural information processing systems*, 32, 2019.

Romain Beaumont. Clip retrieval: Easily compute clip embeddings and build a clip retrieval system with them. `https://github.com/rom1504/clip-retrieval`, 2022.

Sara Beery, Grant Van Horn, and Pietro Perona. Recognition in terra incognita. In *Proceedings of the European conference on computer vision (ECCV)*, pp. 456–473, 2018.

Junbum Cha, Sanghyuk Chun, Kyungjae Lee, Han-Cheol Cho, Seunghyun Park, Yunsung Lee, and Sungrae Park. Swad: Domain generalization by seeking flat minima. In *Advances in Neural Information Processing Systems (NeurIPS)*, 2021.

Junbum Cha, Kyungjae Lee, Sungrae Park, and Sanghyuk Chun. Domain generalization by mutual-information regularization with pre-trained models. *European Conference on Computer Vision (ECCV)*, 2022.

Junhyeong Cho, Gilhyun Nam, Sungyeon Kim, Hunmin Yang, and Suha Kwak. Promptstyler: Prompt-driven style generation for source-free domain generalization. In *Proceedings of the IEEE/CVF International Conference on Computer Vision (ICCV)*, 2023.

Sepehr Dehdashtian, Lan Wang, and Vishnu Naresh Boddeti. Fairerclip: Debiasing zero-shot predictions of clip in rkhss. In *International Conference on Learning Representations*, 2024.

Lisa Dunlap, Yuhui Zhang, Xiaohan Wang, Ruiqi Zhong, Trevor Darrell, Jacob Steinhardt, Joseph E. Gonzalez, and Serena Yeung-Levy. Describing differences in image sets with natural language. In *Conference on Computer Vision and Pattern Recognition (CVPR)*, 2024.

Alex Fang, Gabriel Ilharco, Mitchell Wortsman, Yuhao Wan, Vaishaal Shankar, Achal Dave, and Ludwig Schmidt. Data determines distributional robustness in contrastive language image pre-training (clip). In *International Conference on Machine Learning*, pp. 6216–6234. PMLR, 2022.

Chen Fang, Ye Xu, and Daniel N Rockmore. Unbiased metric learning: On the utilization of multiple datasets and web images for softening bias. In *Proceedings of the IEEE International Conference on Computer Vision*, pp. 1657–1664, 2013.

Stanislav Fort. Pixels still beat text: Attacking the openai clip model with text patches and adversarial pixel perturbations, March 2021. URL `https://stanislavfort.github.io/2021/03/05/OpenAI_CLIP_stickers_and_adversarial_examples.html`.

Yaroslav Ganin, Evgeniya Ustinova, Hana Ajakan, Pascal Germain, Hugo Larochelle, François Laviolette, Mario March, and Victor Lempitsky. Domain-adversarial training of neural networks. *Journal of machine learning research*, 17(59):1–35, 2016.

Ishaan Gulrajani and David Lopez-Paz. In search of lost domain generalization. In *International Conference on Learning Representations*, 2020.

Dan Hendrycks, Steven Basart, Norman Mu, Saurav Kadavath, Frank Wang, Evan Dorundo, Rahul Desai, Tyler Zhu, Samyak Parajuli, Mike Guo, Dawn Song, Jacob Steinhardt, and Justin Gilmer. The many faces of robustness: A critical analysis of out-of-distribution generalization. *ICCV*, 2021.

Gabriel Ilharco, Mitchell Wortsman, Ross Wightman, Cade Gordon, Nicholas Carlini, Rohan Taori, Achal Dave, Vaishaal Shankar, Hongseok Namkoong, John Miller, Hannaneh Hajishirzi, Ali Farhadi, and Ludwig Schmidt. Openclip, July 2021. URL `https://doi.org/10.5281/zenodo.5143773`. If you use this software, please cite it as below.

Pavel Izmailov, Dmitrii Podoprikhin, Timur Garipov, Dmitry Vetrov, and Andrew Gordon Wilson. Averaging weights leads to wider optima and better generalization. *arXiv preprint arXiv:1803.05407*, 2018.

Samyak Jain, Sravanti Addepalli, Pawan Kumar Sahu, Priyam Dey, and R Venkatesh Babu. Dart: Diversify-aggregate-repeat training improves generalization of neural networks. In *Proceedings of the IEEE/CVF Conference on Computer Vision and Pattern Recognition*, pp. 16048–16059, 2023.

Ananya Kumar, Aditi Raghunathan, Robbie Matthew Jones, Tengyu Ma, and Percy Liang. Fine-tuning can distort pretrained features and underperform out-of-distribution. In *International Conference on Learning Representations*, 2021.

Da Li, Yongxin Yang, Yi-Zhe Song, and Timothy M Hospedales. Deeper, broader and artier domain generalization. In *Proceedings of the IEEE international conference on computer vision*, pp. 5542–5550, 2017.

Ziyue Li, Kan Ren, XINYANG JIANG, Yifei Shen, Haipeng Zhang, and Dongsheng Li. SIMPLE: Specialized model-sample matching for domain generalization. In *The Eleventh International Conference on Learning Representations*, 2023. URL `https://openreview.net/forum?id=BqrPeZ_e5P`.

Xiaofeng Mao, Yufeng Chen, Xiaojun Jia, Rong Zhang, Hui Xue, and Zhao Li. Context-aware robust fine-tuning. *International Journal of Computer Vision*, 132(5):1685–1700, 2024.

Prasanna Mayilvahanan, Thaddäus Wiedemer, Evgenia Rusak, Matthias Bethge, and Wieland Brendel. Does CLIP's generalization performance mainly stem from high train-test similarity? In *The Twelfth International Conference on Learning Representations*, 2024. URL `https://openreview.net/forum?id=tnBaiidobu`.

Prasanna Mayilvahanan, Roland S. Zimmermann, Thaddäus Wiedemer, Evgenia Rusak, Attila Juhos, Matthias Bethge, and Wieland Brendel. In search of forgotten domain generalization. In *The Thirteenth International Conference on Learning Representations*, 2025. URL `https://openreview.net/forum?id=Fk3eod9aaD`.

Matthias Minderer, Alexey Gritsenko, and Neil Houlsby. Scaling open-vocabulary object detection. *Advances in Neural Information Processing Systems*, 36:72983–73007, 2023.

Maxime Oquab, Timothée Darcet, Théo Moutakanni, Huy Vo, Marc Szafraniec, Vasil Khalidov, Pierre Fernandez, Daniel Haziza, Francisco Massa, Alaaeldin El-Nouby, et al. Dinov2: Learning robust visual features without supervision. *arXiv preprint arXiv:2304.07193*, 2023.

Xingchao Peng, Qinxun Bai, Xide Xia, Zijun Huang, Kate Saenko, and Bo Wang. Moment matching for multi-source domain adaptation. In *Proceedings of the IEEE/CVF international conference on computer vision*, pp. 1406–1415, 2019.

Alec Radford, Jong Wook Kim, Chris Hallacy, Aditya Ramesh, Gabriel Goh, Sandhini Agarwal, Girish Sastry, Amanda Askell, Pamela Mishkin, Jack Clark, et al. Learning transferable visual models from natural language supervision. In *International conference on machine learning*, pp. 8748–8763. PMLR, 2021.

Alexandre Rame, Matthieu Kirchmeyer, Thibaud Rahier, Alain Rakotomamonjy, Patrick Gallinari, and Matthieu Cord. Diverse weight averaging for out-of-distribution generalization. In *NeurIPS*, 2022.

Benjamin Recht, Rebecca Roelofs, Ludwig Schmidt, and Vaishaal Shankar. Do imagenet classifiers generalize to imagenet? In *International conference on machine learning*, pp. 5389–5400. PMLR, 2019.

Olga Russakovsky, Jia Deng, Hao Su, Jonathan Krause, Sanjeev Satheesh, Sean Ma, Zhiheng Huang, Andrej Karpathy, Aditya Khosla, Michael Bernstein, Alexander C. Berg, and Li Fei-Fei. ImageNet Large Scale Visual Recognition Challenge. *International Journal of Computer Vision (IJCV)*, 115(3):211–252, 2015. doi: 10.1007/s11263-015-0816-y.

Kate Saenko, Brian Kulis, Mario Fritz, and Trevor Darrell. Adapting visual category models to new domains. In *Computer Vision–ECCV 2010: 11th European Conference on Computer Vision, Heraklion, Crete, Greece, September 5-11, 2010, Proceedings, Part IV 11*, pp. 213–226. Springer, 2010.

Christoph Schuhmann, Richard Vencu, Romain Beaumont, Robert Kaczmarczyk, Clayton Mullis, Aarush Katta, Theo Coombes, Jenia Jitsev, and Aran Komatsuzaki. Laion-400m: Open dataset of clip-filtered 400 million image-text pairs. *ArXiv*, abs/2111.02114, 2021. URL `https://api.semanticscholar.org/CorpusID:241033103`.

Yang Shu, Xingzhuo Guo, Jialong Wu, Ximei Wang, Jianmin Wang, and Mingsheng Long. Clipood: Generalizing clip to out-of-distributions. In *International Conference on Machine Learning*, pp. 31716–31731. PMLR, 2023.

Mannat Singh, Laura Gustafson, Aaron Adcock, Vinicius de Freitas Reis, Bugra Gedik, Raj Prateek Kosaraju, Dhruv Mahajan, Ross Girshick, Piotr Dollár, and Laurens Van Der Maaten. Revisiting weakly supervised pre-training of visual perception models. In *Proceedings of the IEEE/CVF Conference on Computer Vision and Pattern Recognition*, pp. 804–814, 2022.

Baochen Sun and Kate Saenko. Deep coral: Correlation alignment for deep domain adaptation. In *Computer Vision–ECCV 2016 Workshops: Amsterdam, The Netherlands, October 8-10 and 15-16, 2016, Proceedings, Part III 14*, pp. 443–450. Springer, 2016.

Piotr Teterwak, Kuniaki Saito, Theodoros Tsiligkaridis, Kate Saenko, and Bryan A Plummer. Erm++: An improved baseline for domain generalization. *arXiv preprint arXiv:2304.01973*, 2023.

Hugo Touvron, Matthieu Cord, Alaaeldin El-Nouby, Jakob Verbeek, and Hervé Jégou. Three things everyone should know about vision transformers. In *European Conference on Computer Vision*, pp. 497–515. Springer, 2022.

Eric Tzeng, Judy Hoffman, Kate Saenko, and Trevor Darrell. Adversarial discriminative domain adaptation. In *Proceedings of the IEEE conference on computer vision and pattern recognition*, pp. 7167–7176, 2017.

Vishaal Udandarao, Ameya Prabhu, Adhiraj Ghosh, Yash Sharma, Philip HS Torr, Adel Bibi, Samuel Albanie, and Matthias Bethge. No" zero-shot" without exponential data: Pretraining concept frequency determines multimodal model performance. *arXiv preprint arXiv:2404.04125*, 2024.

Haohan Wang, Songwei Ge, Zachary Lipton, and Eric P Xing. Learning robust global representations by penalizing local predictive power. In *Advances in Neural Information Processing Systems*, pp. 10506–10518, 2019.

Pengfei Wang, Zhaoxiang Zhang, Zhen Lei, and Lei Zhang. Sharpness-aware gradient matching for domain generalization. In *Proceedings of the IEEE/CVF Conference on Computer Vision and Pattern Recognition*, pp. 3769–3778, 2023.

LI Xuhong, Yves Grandvalet, and Franck Davoine. Explicit inductive bias for transfer learning with convolutional networks. In *International Conference on Machine Learning*, pp. 2825–2834. PMLR, 2018.

Shen Yan, Huan Song, Nanxiang Li, Lincan Zou, and Liu Ren. Improve unsupervised domain adaptation with mixup training. *arXiv preprint arXiv:2001.00677*, 2020.

Han Yu, Xingxuan Zhang, Renzhe Xu, Jiashuo Liu, Yue He, and Peng Cui. Rethinking the evaluation protocol of domain generalization. In *Proceedings of the IEEE/CVF Conference on Computer Vision and Pattern Recognition*, pp. 21897–21908, 2024.

Zhun Zhong, Yuyang Zhao, Gim Hee Lee, and Nicu Sebe. Adversarial style augmentation for domain generalized urban-scene segmentation. *Advances in Neural Information Processing Systems*, 35:338–350, 2022.

A Appendix

A.1 Training and Evaluation Details

We use a slightly modified MIRO (Cha et al., 2022) codebase for training and evaluation. We use **leave-one-out** evaluation, where a model is trained on all domains except the evaluation domain. We emphasize that we use DomainBed-IP and DomainBed-OOP as evaluation data only, models are trained on full datasets.

For training, we use an OpenCLIP-ViT-B/16 (Ilharco et al., 2021) trained on LAION-400M (Schuhmann et al., 2021). We use default hyper-parameters as defined by (Cha et al., 2022). This includes a learning rate of 5e-5, weight decay of 0.0, a batch size of 32 per-domain, an Adam Optimizer, and no dropout for all methods.

For evaluation, unlike DomainBed, we consider the entire test domain instead of an 80% random split. Following standard practice, we first compute accuracy for each domain, then average those accuracies to get dataset level statistics, and finally compute overall averages averaging across datasets.

For benchmarked methods, we also use hyper-parameters found to be best in respective papers. For **SWAD**, we use an optimum patience parameter value of 3, overfit patience parameter value of 6, and tolerance ratio of 6. For **MIRO**, we use use regularizer loss weight of 1.0. For **CORAL**, we use a CORAL regularizer weight of 1.0, following (Cha et al., 2021). For **LP-FT**, we train the linear probe for 600 steps before unlocking the full backbone. For **Model Parameter Averaging**, we burn in the training for 600 steps before averaging iterates. For **VL2V-SD** and **CLIPood**, we directly use the author's implementation and hyper-parameters, except initializing with OpenCLIP (Ilharco et al., 2021).

A.2 Training Compute

Each run uses an A6000 48GB GPU, trained for up to 12 hours per domain-dataset combination.

B Additional Results

B.1 AlignmentScore vs Accuracy

In Figure 11, we plot all benchmarked methods from the main paper, with x-axis corresponding to AlignmentScore, and the y-axis corresponding to the Top-1 Accuracy. We normalize for dataset size, so that no dataset dominates the count. In Figures 12 through 16, we plot these statistics independently per dataset, and find the trends consistent across datasets.

B.2 Per-Dataset Benchmarking Results

We expand Table 1 in the main paper into per-dataset results in Table 10 through 24.

B.3 Similarity of Target to Pre-training

To evaluate the Image Similarity Hypothesis, we retrieve the nearest neighbors from the Laion-400M dataset (Schuhmann et al., 2021). This raises the question of how similar the target domains are to

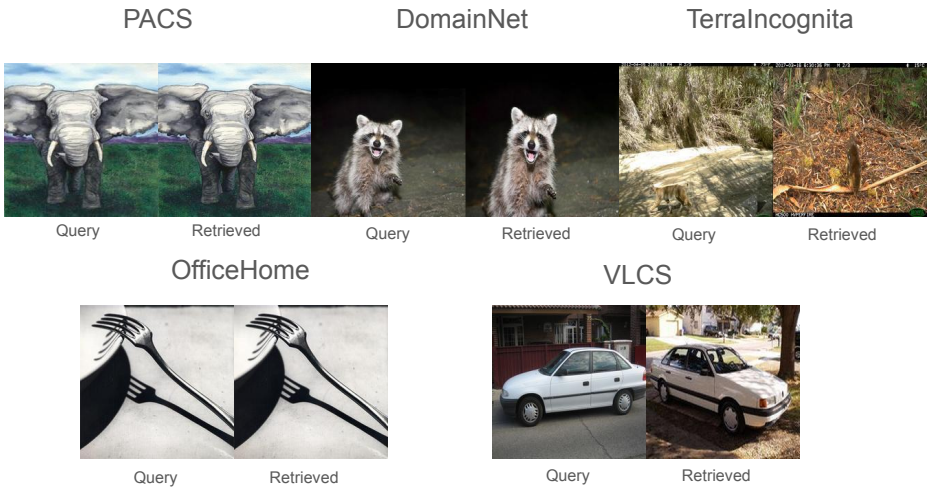

Figure 4: Nearest neighbors of target images in pre-training LAION data.

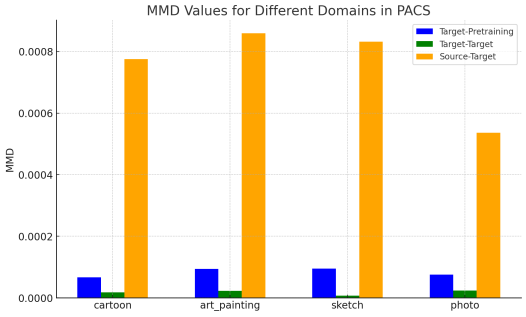

Figure 5: MMD between pre-training and target, source and target, and target and target for PACS. Target is more similar to pre-training than source. Despite this, Alignment is a better predictor of DG performance than perceptual similarity.

the pre-training data and whether the source domains might be even more similar. To investigate this, we compute Maximum Mean Discrepancy (MMD) distances between PACS domains and their nearest neighbors from Laion-400M, as shown in Figure 5. Our results indicate that target domains are, in fact, more similar to the pre-training data than source domains. We inspect nearest neighbors manually, and find even exact duplicates (Figure 4). Interestingly, while we found not only domain-level duplicates but also exact matches in the pre-training data, the Image Similarity Hypothesis is ultimately less predictive than the Alignment Hypothesis.

B.4 Other backbones

We benchmark 2 additional backbones(DINOv2 (Oquab et al., 2023) and OpenAI CLIP) using the MIRO + MPA Domain Generalization method, which we found to be the strongest in our paper, on two datasets (OfficeHome and PACS). This consistency is likely due to the similar nature of the pre-training datasets, both sourced from web scraping and of comparable scale. These findings reinforce that the usefulness of the DomainBed-IP/OOP split is not confined to a specific backbone.

Table 2: Benchmark results of different backbones on OfficeHome and PACS datasets.

Backbone	**OfficeHome - IP**	**PACS - IP**	**OfficeHome - OOP**	**PACS - OOP**
OpenCLIP-ViT/B 16	90.7	98.1	60.0	87.8
CLIP-ViT/B 16	88.1	97.6	57.0	86.9
DinoV2	87.4	97.1	58.9	85.0

Table 3: Splitting DomainBed by PerceptualSimilarityScore. The differences between IP and OOP with this split are much lower than with Alignment Score.

Dataset	PACS	VLCS	TerraIncognita	OfficeHome	DomainNet
Perceptual IP	97.2	74.8	60.6	86.8	61.4
Perceptual OOP	95.6	77.4	42.9	78.3	55.3

B.5 SPLITTING DOMAINBED USING PERCEPTUALSIMILARITYSCORE

In Figure 2 b.), we show that the slope of the relationship of Top-1 Accuracy vs Perceptual Similarity Score is positive but shallow. This suggests that using PerceptualSimilarityScore as an alternative to AlignmentScore for splitting DomainBed would not be very effective. To further prove this point, we split at a PerceptualSimilarityScore value of 0.86 in Table 3. We can see the differences are not very large between OOP and IP, indicating that AlignmentScore is a better thresholding metric.

B.6 COMPARING ALIGNMENTSCORE WITH ZERO-SHOT CLASSIFICATION CONFIDENCE SCORE

We also consider an alignment score which takes into account uncertainties, and compute a score using the confidence of the zero-shot classifier formed by the pre-trained CLIP model for each sample. Specifically, for a sample with ground truth class c, we calculate the softmax over the logits output by the zero-shot classifier, and use the resulting probability p(c) as the score. We refer to this as the Calibrated AlignmentScore and show the results in Figure 6. Although the score predicts generalization for both OfficeHome and DomainNet, the scores have different scales for different datasets. In contrast out AlignmentScore does align across datasets to a greater degree (Figure 7)

We explore the effect of averaging PerceptualSimilarityScore and AlignmentScore in Figure 8. We can see that there is not much of a compositional effect, so therefore we stick with AlignmentScore as our generalization predictor.

B.7 IMAGE SIMILARITY HYPOTHESIS FOR SOURCE DATA

The main drawback of the Image Similarity hypothesis is that it does not consider how well the nearest perceptual neighbor is learned during pre-training. One reason for a sample being poorly learned during pre-training is that the pre-training caption is not very relevant to the DG task. Source data is unlikely to have this issue, since source and target domains share labels. Therefore it is interesting to ask how strongly correlated the PerceptualSimilarityScore is with DG accuracy when measured between source and target. Indeed , as seen in Figure 9, there is a strong correlation. However, simply using source-data to compute the PerceptualSimilarity results in an incomplete understanding of the relationship between target data and the training procedure, due to the lack of consideration of the pre-training. In fact, zero-shot models with NO learning from source are very performant (Table 1)

B.8 TRAINING FROM SCRATCH

We focus on analyzing the generalization capabilities of CLIP-based DG methods, as these have been demonstrated to be the strongest in recent work. However,from-scratch experiments are valuable to measure how much finetuning on source data can learn, and so we also trained ResNet-50 models from scratch, using the MPA (Model Parameter Averaging) method and present the results in Table 4. We can see that performance is very low even on ALL DomainBed data (unsplit), further

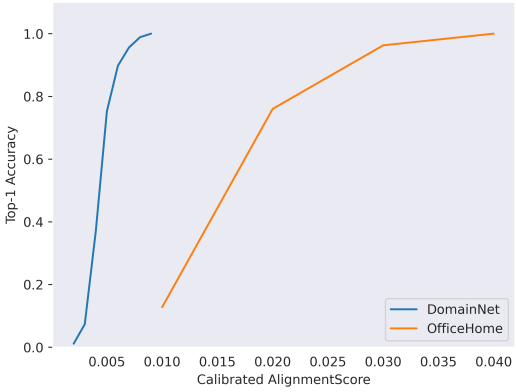

Figure 6: Top-1 DG Accuracy vs calibrated alignment: We use the confidence of the zero-shot classifier formed by the pre-trained CLIP models an alignment measure. Although the score predicts generalization for both OfficeHome and DomainNet, the scores have different scales for different datasets.

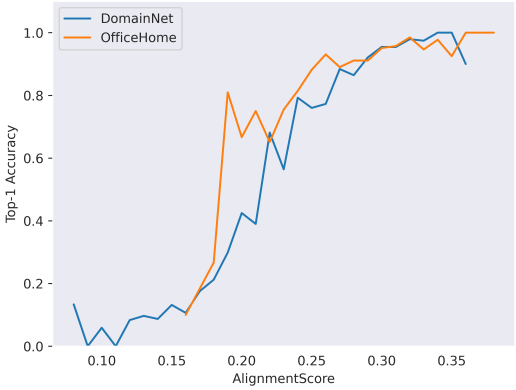

Figure 7: Top-1 DG Accuracy vs AlignmentScore: The AlignmentScore introduced in our work have scales which are comparable across different datasets.

confirming that existing DG algorithms are poor at learning new knowledge from source data alone, and they rely on strong pre-training for good performance.

B.9 Analysis of Zero-Shot Behavior

To better understand the behavior of Domain Generalization (DG) methods, we compute confusion matrices for zero-shot (ZS) and In-Pretraining (IP) and Out-of-Pretraining (OOP) subsets for the PACS dataset using CLIPood. The results are shown in Tables 5 and 6.

The confusion matrices reveal key insights about the behavior of DG methods:

- For the **IP subset**, DG methods catastrophically forget a significant number of samples, flipping correct predictions made by zero-shot models to incorrect ones. This suggests that DG methods can even have a *negative value* for IP data. Nevertheless, performance remains strong.
- For the **OOP subset**, DG methods flip very few correct samples to incorrect ones. However, the state-of-the-art (SOTA) method, CLIPood, is still unable to correct the majority of incorrectly classified samples in this subset.

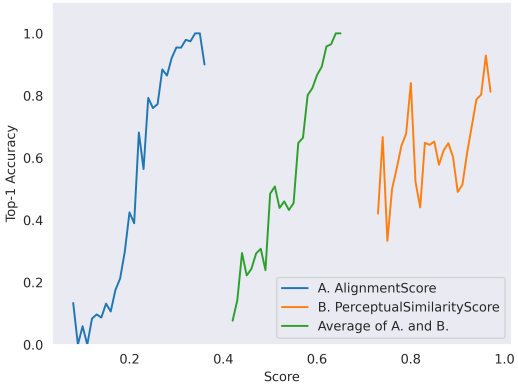

Figure 8: Combining PerceptualSimilarity Score and AlignmentScore: We explore the effect of averaging PerceptualSimilarityScore and AlignmentScore. There is no visible additional signal from averaging. We therefore stick with AlignmentScore as our generalization predictor.

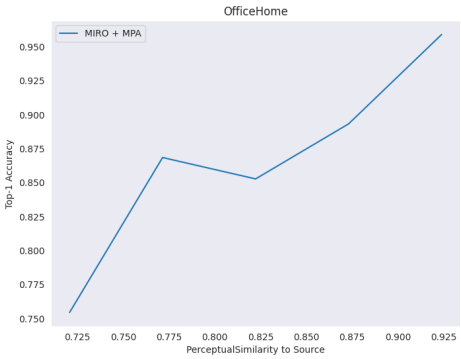

Figure 9: PerceptualSimilarity to Source for OfficeHome. DG performance is correlated with similarity to source images.

Overall, in both IP and OOP cases, the results indicate that CLIPood and other DG methods rely heavily on pre-training. These findings underscore the limitations of current DG methods and highlight areas for improvement.

C Additional DomainBed-(IP/OOP) Statistics and Analysis

C.1 Constituent Datasets

We split 5 datasets in DomainBed-(IP/OOP),(VLCS (Fang et al., 2013), DomainNet (Peng et al., 2019), OfficeHome (Ganin et al., 2016), PACS (Li et al., 2017), and TerraIncognita (Beery et al., 2018)). Here we provide basic statistics of each.

VLCS has 5 classes and 4 domains: Caltech101, LabelME, SUN09, and VOC2007, with 10729 samples. The domain shift is dataset source.

DomainNet contrains 345 classes and 6 domains: clipart, infograph, quickdraw, real, and sketch. It has a total of 586,575 samples. The dataset shift is style.

OfficeHome has 65 classes and 4 domains: art, clipart, product, and real. The dataset shift is style.

TerraIncognita has 10 classes of wildlife cameras. There are 4 domains of different cameras and 24788 samples. The dataset shift is camera location.

Table 4: Training ResNet-50 from scratch. DG performance is very poor, showing DG methods rely on strong pre-training

	DomainNet	OfficeHome	PACS	TI	VLCS	Avg
ResNet-50 from Scratch	7.6	17.2	36.3	23.8	55.2	28.0
Clip ViT-B/16	58.9	82.0	94.3	50.7	82.3	73.6

Table 5: Confusion matrix for the IP subset of the PACS dataset.

	DG: Incorrect	**DG: Correct**
ZS: Incorrect	141	70
ZS: Correct	179	8231

PACS has 9991 sampes and 4 domains: arts, cartoon, photo, and sketch. There are 7 classes. The dataset shift is style.

C.2 Mislabeling and OCR Rates

In Table 7 we present the mislabelling rates at various AlignmentScore values. In Table 8, we present how much data is removed due to mislabelling or OCR filtering.

C.3 Class Distribution of DomainBed-(IP/OOP):

In Figures 19 through 33, we provide class distribution statistics of different datasets before splitting and in our IP and OOP splits. We find some interesting patterns. For example, in Office-Home, the OOP class is dominated by **marker** and **toys**, while the IP split has a much more uniform distribution. Similarly, both PACS (DomainBed-OOP) and VLCS (DomainBed-OOP) are dominated by **person**.

C.4 VisDiff differences between DB-IP and DB-OOP

We further investigate the distinctions between the IP and OOP subsets using VisDiff (Dunlap et al., 2024), an LLM-based system that identifies differences between sets of images. For each combination of dataset, domain, and class—except for DomainNet, where we subsample roughly 15% of the combinations due to computational constraints—we independently sample up to 30 images from both the IP and OOP subsets. VisDiff employs CLIP to compute an AUC-ROC score for the natural language differences proposed by the LLM, and we retain only those differences with an AUC score of 0.7 or higher. The complete results are presented in Table 9.

C.5 Relationship between object size and AlignmentScore

To test whether object size is correlated with AlignmentScore, we computed the object size of the ground truth labeled objects using bounding boxes generated by the open-world object detector OWLv2 (Minderer et al., 2023). Overall, object size is correlated with the AlignmentScore (see Figure 10), with the sole exception being the TerraIncognita dataset. This indicates that even the presence of small wildlife can substantially increase the AlignmentScore, and that the background vegetation does not present a significantly conflicting signal that is sometimes present in other datasets. Overall, this suggests that pre-training which better represents scenes with multiple objects or concepts may improve benchmark performance.

Table 6: Confusion matrix for the OOP subset of the PACS dataset.

	DG: Incorrect	**DG: Correct**
ZS: Incorrect	98	62
ZS: Correct	15	890

Table 7: Mislabeling rates across different AlignmentScore ranges.

Dataset	0.0-0.05	0.05-0.10	0.10-0.15	0.15-0.20
OfficeHome	100%	45%	28%	12%
PACS	-	46%	5%	0%
TerraIncognita	-	55%	34%	23%
DomainNet	65%	35%	33%	11%
VLCS	33%	14%	9%	3%

Table 8: Percentage of discarded samples due to mislabeling or label text in the image (OCR).

Dataset	**Dropped - Mislabelled**	**Dropped - OCR**
OfficeHome	0.92%	0.15%
PACS	3.05%	0.00%
TerraIncognita	0.22%	0.00%
DomainNet	7.64%	0.03%
VLCS	12.41%	0.00%

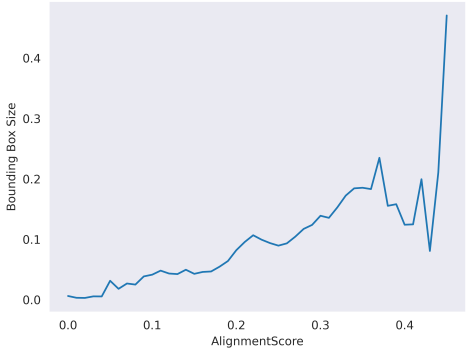

(a) All datasets.

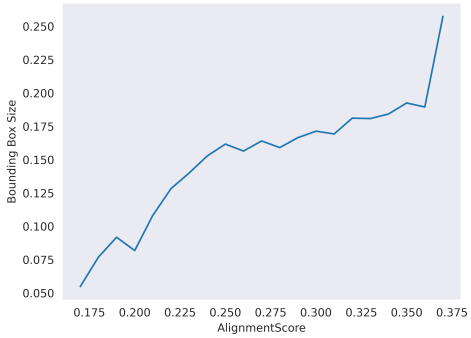

(b) OfficeHome.

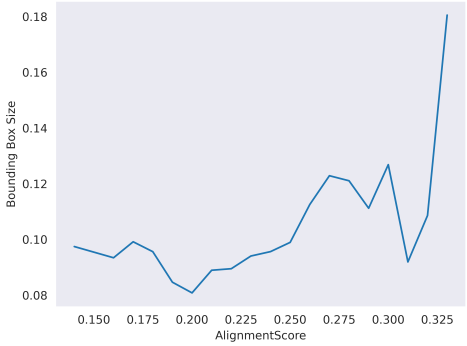

(c) PACS.

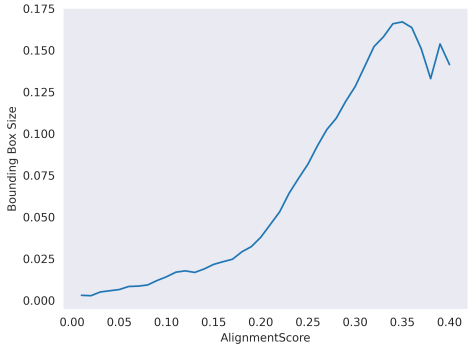

(d) DomainNet.

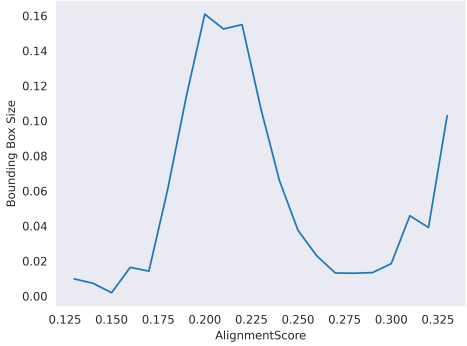

(e) TerraIncognita.

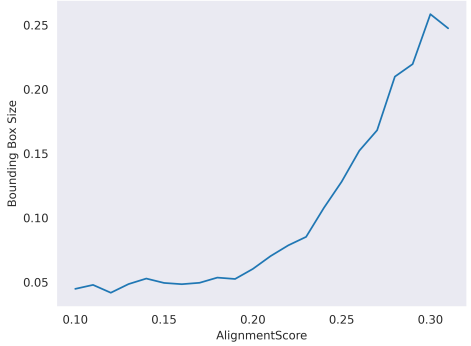

(f) VLCS.

Figure 10: Overall relationship between ground truth object bounding box size and AlignmentScore across different DomainBed datasets. Overall the relationship is positive, indicating that object size plays a role in whether a data point is IP or OOP. The exception is TerraIncognita, indicating that camera trap backgrounds do not strongly conflict with the presence of the wildlife to be classified. See Section C.5.

Table 9: VisDiff: Differences Identified for Image Sets. We use VisDiff (Dunlap et al., 2024), an LLM-based system for describing differences between images sets, to identify differences in between IP and OOP images. We do so independently for each dataset, domain, and class grouping. Distractors unrelated to the class seem to be an issue. For more details see Section C.4.

Dataset_Domain_Class	**Description**
VLCS_SUN09_car	Historical architecture
VLCS_SUN09_bird	variety of landscapes
VLCS_SUN09_person	indoor water parks
VLCS_Caltech101_dog	text about adoption and rescue services
VLCS_LabelMe_chair	people walking on city streets
VLCS_LabelMe_dog	gatherings of people
VLCS_Caltech101_bird	paintings
VLCS_Caltech101_person	murals on buildings
VLCS_VOC2007_dog	inside homes with multiple people
VLCS_Caltech101_car	presence of branded vehicles
VLCS_SUN09_dog	cooking areas
VLCS_VOC2007_car	double decker buses
VLCS_LabelMe_bird	people near bodies of water
VLCS_VOC2007_person	equestrian activities
VLCS_VOC2007_bird	people engaging in activities
terra_incognita_location_38_rabbit	sunny daytime scenes
terra_incognita_location_38_squirrel	streams in wooded areas
terra_incognita_location_46_opossum	animal walking
terra_incognita_location_100_dog	muddy areas
terra_incognita_location_46_raccoon	cloud formations
terra_incognita_location_43_dog	streams in the forest
terra_incognita_location_100_bird	a dirt road in a garden
terra_incognita_location_46_squirrel	camera trap captures
terra_incognita_location_38_bird	night vision
terra_incognita_location_46_empty	middle of the night
terra_incognita_location_100_rabbit	absence of man-made objects
terra_incognita_location_38_opossum	screens with green backgrounds
terra_incognita_location_46_dog	crocodiles
terra_incognita_location_46_rabbit	shadows in nature
terra_incognita_location_100_squirrel	dirt roads
terra_incognita_location_38_cat	a black bear resting on a log
terra_incognita_location_43_squirrel	muddy areas
terra_incognita_location_43_bobcat	an image of a crocodile
terra_incognita_location_43_bird	deserts
terra_incognita_location_38_coyote	black bears
terra_incognita_location_46_bobcat	streams in a wooded area
terra_incognita_location_46_coyote	waterfalls
terra_incognita_location_46_cat	Wooded areas
terra_incognita_location_43_coyote	crocodiles
terra_incognita_location_43_opossum	boats in water
terra_incognita_location_100_cat	images of tapirs at night
terra_incognita_location_100_raccoon	natural landscape
terra_incognita_location_43_cat	animals resting
terra_incognita_location_43_raccoon	wildlife in water
office_home_Art_Paper_Clip	animals hanging
office_home_Clipart_Webcam	colorful backgrounds
office_home_Product_Soda	rows of multiple beverage containers
office_home_Real_Speaker	jbl portable bluetooth speakers
office_home_Product_Drill	yellow and black color scheme
office_home_Real_Clipboards	advertising signage

Table 9

Dataset_Domain_Class	**Description**
office_home_Clipart_Fan	close-up views
office_home_Real_Bike	road cycling
office_home_Product_Lamp_Shade	circular objects
office_home_Clipart_Notebook	textbooks with colorful covers
office_home_Real_Sink	brushed nickel finish
office_home_Clipart_Keyboard	singular computer components
office_home_Art_Speaker	toy-like objects
office_home_Product_Radio	bluetooth devices
office_home_Real_Glasses	space-related elements
office_home_Clipart_Desk_Lamp	asian clothing styles
office_home_Art_Bottle	earrings with a bottle and cork
office_home_Clipart_Clipboards	a promotional offer
office_home_Real_Flowers	butterflies
office_home_Product_Fan	air purifiers
office_home_Clipart_Alarm_Clock	cartoon characters
office_home_Art_Backpack	toys with wings
office_home_Art_Computer	illustrations
office_home_Art_Shelf	flowers in pots
office_home_Product_Pen	focus on packaging
office_home_Product_Mouse	colorful electronics on display
office_home_Clipart_Postit_Notes	notebooks on a table
office_home_Product_Clipboards	natural materials without additional items
office_home_Product_Batteries	set of six objects
office_home_Clipart_Curtains	feminine imagery
office_home_Art_Pan	eggs with faces drawn on them
office_home_Clipart_Telephone	3D rendering
office_home_Clipart_Monitor	technology themes
office_home_Product_Screwdriver	close-up of a person engaged in an activity
office_home_Clipart_Paper_Clip	Red color prominence
office_home_Product_Calendar	octagon shapes
office_home_Product_Couch	close-up furniture shots
office_home_Art_Helmet	dragon's head
office_home_Clipart_File_Cabinet	3D rendering
office_home_Clipart_Shelf	commercial products
office_home_Clipart_TV	realistic images
office_home_Real_Curtains	a bathroom setting
office_home_Art_Toys	a small white dog
office_home_Art_Glasses	individual with headgear
office_home_Product_Sneakers	gel cushioning
office_home_Real_Drill	blue colored objects
office_home_Clipart_Glasses	audio equipment
office_home_Clipart_Lamp_Shade	black and white drawing
office_home_Real_Bed	child-themed decor
office_home_Art_File_Cabinet	people in a professional setting
office_home_Product_Backpack	focus on material texture
office_home_Art_Printer	office settings with unusual elements
office_home_Real_Batteries	emphasis on a specific brand
office_home_Art_Soda	cans of angry birds tropic soda
office_home_Real_Trash_Can	objects on wheels
office_home_Product_Eraser	packages explicitly labeled 'pentel'
office_home_Real_Shelf	laundry room
office_home_Clipart_Eraser	book on a black background
office_home_Clipart_ToothBrush	distinctive backgrounds
office_home_Product_Glasses	sunglasses with red lenses
office_home_Clipart_Calendar	sanitation theme

Table 9

Dataset_Domain_Class	Description
office_home_Clipart_Mop	detailed human figures
office_home_Art_Oven	combination of domestic and clinical spaces
office_home_Real_Lamp_Shade	minimalist style
office_home_Art_Fan	digital artwork
office_home_Art_Webcam	futuristic design
office_home_Art_Laptop	fantasy or fictional themes
office_home_Art_Bed	enchantment
office_home_Art_Curtains	dark hair
office_home_Real_Fan	multiple ceiling fans
office_home_Clipart_Pen	cocktail shakers
office_home_Art_Screwdriver	blue and silver color palette
office_home_Product_Keyboard	gaming mouse included
office_home_Real_Notebook	colorful stationery
office_home_Real_Couch	contemporary living spaces
office_home_Art_Table	standing posture
office_home_Art_Pen	creative process
office_home_Real_Mop	clothes hanging
office_home_Art_Scissors	video game characters
office_home_Clipart_Scissors	abstract shapes
office_home_Art_Keyboard	concrete structures
office_home_Real_Calendar	printable charts with decorative backgrounds
office_home_Art_Calculator	decorative elements
office_home_Art_Bike	animal on a vehicle
office_home_Product_Webcam	a single computer monitor
office_home_Clipart_Bottle	household container
office_home_Clipart_Computer	a printer
office_home_Real_Sneakers	Black high top sneakers
office_home_Clipart_Mouse	monochromatic themes
office_home_Art_Notebook	objects with a vintage look
office_home_Clipart_Bucket	objects associated with liquids
office_home_Product_Laptop	abstract simplicity
office_home_Art_Push_Pin	digital art
office_home_Real_Push_Pin	objects placed against natural backgrounds
office_home_Art_Ruler	animal skulls
office_home_Art_Couch	cats
office_home_Art_Desk_Lamp	intricate costumes
office_home_Art_Mouse	unique artistic interpretations
office_home_Art_Refrigerator	a toy girl in an unusual setting
office_home_Product_Knives	survival or tactical items
office_home_Product_Helmet	an image of a protective gear
office_home_Clipart_Helmet	abstract concepts
office_home_Product_Notebook	calendar
office_home_Product_Paper_Clip	a caliper and a paper clip
office_home_Product_Hammer	hammer head detail
office_home_Clipart_Bed	detailed human emotions
office_home_Clipart_Chair	a red background
office_home_Art_Flowers	cakes with unique decorations
office_home_Product_Toys	White and brown plush toys
office_home_Art_Fork	red dress
office_home_Real_Pan	cooked fish
office_home_Real_Bucket	tabletop settings
office_home_Art_Trash_Can	drinks on a colorful background
office_home_Real_Knives	focus on object
office_home_Real_Pencil	pink color theme
office_home_Product_File_Cabinet	green objects on a white background

Table 9

Dataset_Domain_Class	**Description**
office_home_Real_Hammer	German craftsmanship
office_home_Art_Sink	illustrations
office_home_Clipart_Screwdriver	minimalistic design
office_home_Art_Marker	illustrations of animals
office_home_Art_Telephone	sport equipment
office_home_Real_Folder	blue wall
office_home_Product_Folder	focus on texture
office_home_Clipart_Batteries	objects on a plain, uncluttered background
office_home_Product_Mug	black handle
office_home_Product_Flowers	a single red rose
office_home_Real_Soda	mango juice with a straw
office_home_Art_Lamp_Shade	people with hats
office_home_Clipart_Oven	focus on a single object
office_home_Art_Spoon	fantasy elements
office_home_Clipart_Table	cartoons
office_home_Clipart_Hammer	food items
office_home_Art_Radio	yellow boomboxes
office_home_Clipart_Sink	human activity
office_home_Clipart_Drill	digital art style
office_home_Art_Eraser	illustrations or drawings
office_home_Clipart_Exit_Sign	clear and singular message
office_home_Clipart_Pencil	a spool of ribbon
office_home_Art_Batteries	graphic t-shirts
office_home_Art_Mug	coffee with food items inside
office_home_Clipart_Bike	signs with text
office_home_Art_TV	multiple tv screens
office_home_Product_Chair	inflatable furniture
office_home_Art_Drill	conceptual illustrations
office_home_Art_Postit_Notes	cookies
office_home_Art_Chair	fire or flames
office_home_Art_Hammer	women in fantasy attire
office_home_Art_Folder	men in suits
office_home_Product_Computer	MSI branded devices
office_home_Product_Push_Pin	geographic representations
office_home_Clipart_Laptop	a pair of devices
office_home_Art_Sneakers	octopuses on shoes
office_home_Art_Candles	whimsical objects
office_home_Real_Chair	ottomans
office_home_Clipart_Pan	stacked objects
office_home_Art_Bucket	man playing music
PACS_cartoon_person	images featuring ice cream
PACS_art_painting_dog	hunting scenes
PACS_art_painting_giraffe	deer in the artwork
PACS_art_painting_guitar	artwork displaying paint splatters
PACS_art_painting_person	artistic depictions featuring abstract or imaginative elements
PACS_cartoon_horse	giraffes
PACS_cartoon_guitar	hand-drawn illustrations
PACS_photo_dog	dogs in vehicles
PACS_photo_horse	non-living objects
PACS_art_painting_horse	bulls
domain_net_clipart_shorts	characters with speech bubbles
domain_net_infograph_bottlecap	technical illustrations
domain_net_infograph_kangaroo	different types of fish in infographics

Table 9

Dataset_Domain_Class	Description
domain_net_clipart_bicycle	scenes involving flight
domain_net_sketch_sock	monkeys as a subject
domain_net_painting_stethoscope	text with humor or messages
domain_net_infograph_aircraft_carrier	an organized visual representation of navy ships
domain_net_clipart_The_Eiffel_Tower	black background
domain_net_sketch_submarine	educational elements like drawing guides
domain_net_clipart_parrot	blue birds
domain_net_painting_string_bean	paintings on a striped background
domain_net_real_house	large resorts
domain_net_real_stop_sign	images near a river
domain_net_clipart_mouse	cute small animals
domain_net_real_hedgehog	objects in a grassy area
domain_net_real_cat	presence of dogs
domain_net_painting_bucket	watercolor paintings
domain_net_sketch_motorbike	steampunk design
domain_net_sketch_wine_glass	cocktails
domain_net_painting_strawberry	lace tablecloths
domain_net_sketch_bus	text elements in illustrations
domain_net_infograph_flower	floral arrangements
domain_net_clipart_tiger	Airplanes flying in the sky
domain_net_clipart_lobster	repeated phrases or words
domain_net_sketch_baseball	a basketball on a wooden floor
domain_net_infograph_steak	comparison charts
domain_net_sketch_pillow	teddy bear motifs
domain_net_clipart_fish	black and white illustrations
domain_net_infograph_hockey_puck	infographics focusing on player statistics
domain_net_painting_bandage	children in art
domain_net_painting_harp	circular tables
domain_net_sketch_ant	clouds
domain_net_sketch_calculator	squares and shapes
domain_net_sketch_church	specific locations
domain_net_infograph_paintbrush	informative visual aids
domain_net_painting_sea_turtle	stained glass
domain_net_clipart_candle	birthday-themed images
domain_net_clipart_baseball_bat	characters with beverages
domain_net_painting_squirrel	a combination of different artistic styles
domain_net_infograph_trumpet	mushrooms
domain_net_real_cloud	illustrations of devices
domain_net_infograph_string_bean	dairy farm flyer
domain_net_clipart_scorpion	designs for personal adornment
domain_net_painting_mouth	art creation process
domain_net_painting_pickup_truck	people creating art
domain_net_painting_scorpion	paintings with multiple subjects
domain_net_clipart_asparagus	chef's hat
domain_net_real_elephant	frogs
domain_net_painting_suitcase	scenes involving rivers or water
domain_net_real_tornado	a video game setting
domain_net_painting_pond	a painting of people
domain_net_painting_oven	indoor car scenes
domain_net_infograph_flip_flops	modern info presentation template
domain_net_clipart_vase	casual outdoors
domain_net_clipart_dolphin	multiple animal species
domain_net_real_lightning	people indoors
domain_net_infograph_banana	recipes

Table 9

Dataset_Domain_Class	Description
domain_net_painting_cooler	incomplete words on objects
domain_net_sketch_tractor	depiction of people
domain_net_clipart_power_outlet	colorful graphic design
domain_net_infograph_bandage	infographics
domain_net_real_string_bean	recipes with bacon
domain_net_infograph_sheep	leather industry
domain_net_real_carrot	hummus
domain_net_painting_lighthouse	murals
domain_net_clipart_skyscraper	flyer designs
domain_net_sketch_blueberry	a set of hand drawn fruit
domain_net_sketch_snorkel	cartoon animals
domain_net_infograph_vase	flyers with promotional content
domain_net_real_moon	mythological or fantasy elements
domain_net_sketch_hamburger	fast food with ice cream
domain_net_infograph_barn	organic farming elements
domain_net_clipart_rainbow	umbrellas
domain_net_clipart_dog	images featuring human characters
domain_net_infograph_elbow	educational posters
domain_net_clipart_face	vector illustrations
domain_net_sketch_hourglass	vector illustrations
domain_net_sketch_laptop	people sitting at desks
domain_net_real_fire_hydrant	airplane in the sky
domain_net_real_mouse	a cable connection
domain_net_real_hourglass	jewelry
domain_net_painting_whale	paintings in a gallery setting
domain_net_painting_envelope	mixed media paintings
domain_net_sketch_flip_flops	illustrations of hats and sunglasses
domain_net_infograph_hedgehog	infographics with statistical data
domain_net_painting_sun	depictions of solitude
domain_net_painting_knee	military uniforms
domain_net_clipart_butterfly	birds and flowers
domain_net_sketch_goatee	illustrations of chefs
domain_net_real_airplane	dynamic outdoor sports
domain_net_sketch_banana	hand drawn illustrations
domain_net_infograph_lollipop	sweet-themed infographics
domain_net_real_owl	colorful designs
domain_net_real_banana	plate presentations
domain_net_painting_tornado	people in colorful dresses
domain_net_real_lobster	multiple dishes presented together
domain_net_sketch_frog	people drawing with different tools
domain_net_real_mountain	extreme sports
domain_net_real_drums	guitar
domain_net_infograph_knee	recovery processes
domain_net_real_teapot	coffee mugs
domain_net_real_camouflage	images with helicopters
domain_net_infograph_parrot	first aid themes
domain_net_infograph_bathtub	wheelchair-accessible features
domain_net_painting_bracelet	artistic portraits
domain_net_painting_fireplace	people sitting together
domain_net_sketch_owl	Rough outlines
domain_net_sketch_crocodile	lizards and frogs
domain_net_clipart_kangaroo	Christmas themes
domain_net_clipart_cat	cartoons with both cats and dogs
domain_net_real_golf_club	screenshots of video games
domain_net_painting_laptop	illustrated people

Table 9

Dataset_Domain_Class	**Description**
domain_net_clipart_broom	dog in a witch's hat with a pumpkin
domain_net_painting_bulldozer	night scenes indoors
domain_net_sketch_sailboat	nautical-themed accessories
domain_net_clipart_picture_frame	Colorful paw prints
domain_net_clipart_octagon	colorful gumballs
domain_net_clipart_ladder	whimsical illustrations
domain_net_clipart_scissors	illustrations with human figures
domain_net_clipart_tractor	images of airplanes
domain_net_real_chandelier	rooms with large beds
domain_net_sketch_guitar	Everyday scenes involving musical themes
domain_net_clipart_broccoli	promotional style imagery
domain_net_clipart_ice_cream	refrigerators
domain_net_painting_octagon	birds
domain_net_clipart_church	ceremonial events
domain_net_infograph_sleeping_bag	child safety
domain_net_painting_drill	colorful outdoor scenes
domain_net_painting_hot_tub	green character in a bathroom scene
domain_net_clipart_rhinoceros	cartoon characters
domain_net_sketch_roller_coaster	people on a piece of paper
domain_net_painting_bridge	Venice
domain_net_clipart_violin	animals playing instruments
domain_net_real_mosquito	abstract or surreal elements
domain_net_sketch_spider	comic book grading
domain_net_infograph_donut	checkered patterns
domain_net_painting_stairs	art restoration
domain_net_clipart_flamingo	patterns and designs
domain_net_real_knee	people in stylish outfits
domain_net_infograph_basketball	detailed sports statistics
domain_net_clipart_sleeping_bag	colorful designs
domain_net_painting_remote_control	watercolor
domain_net_painting_calculator	a person multitasking
domain_net_real_speedboat	tourist beaches
domain_net_clipart_bus	psychedelic imagery
domain_net_painting_speedboat	images with a variety of painting mediums
domain_net_painting_toilet	decorative art
domain_net_painting_cell_phone	colorful designs
domain_net_sketch_beard	scenes depicting historical or fictional characters
domain_net_clipart_key	a man in a hat
domain_net_clipart_spreadsheet	vector illustrations with folders
domain_net_infograph_mushroom	identification charts
domain_net_clipart_nose	cartoon animal with a flower
domain_net_painting_stop_sign	oil paintings
domain_net_sketch_baseball_bat	vector illustrations on a black background
domain_net_real_elbow	colorful clothing
domain_net_infograph_feather	posters for events
domain_net_clipart_dragon	an airplane flying

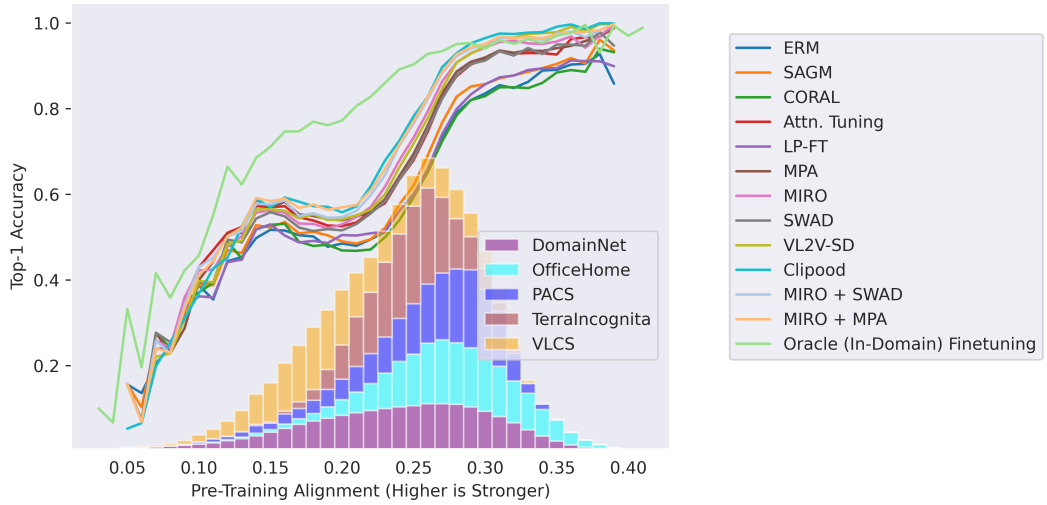

Figure 11: Plotting AlignmentScore vs Top-1 Accuracy for all benchmarked methods, for all datasets together. Although some methods are stronger than others, all follow the same trend of increasing accuracy with increased AlignmentScore.

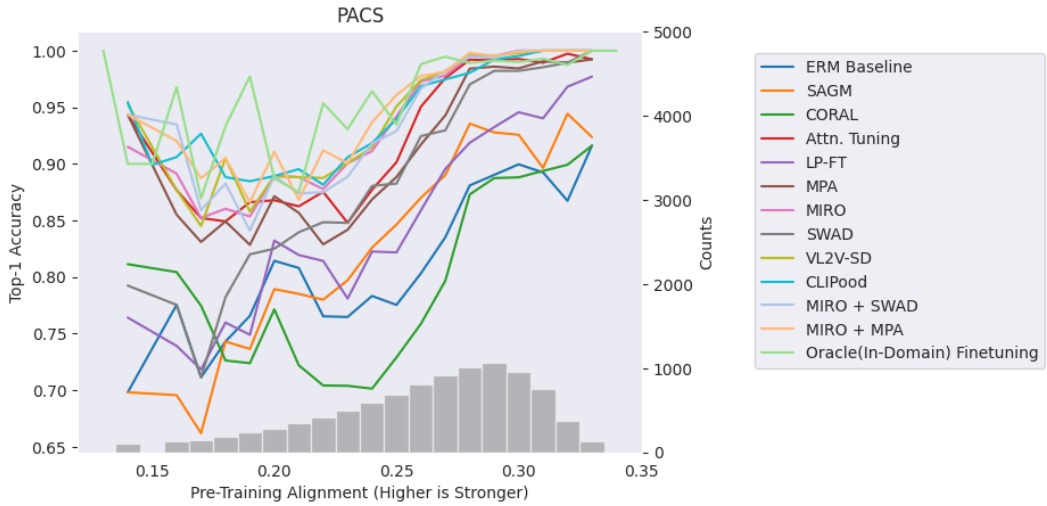

Figure 12: Plotting AlignmentScore vs Top-1 Accuracy on the PACS dataset.

Table 10: Per-domain breakdown for OfficeHome (DomainBed-OOP)

Method	Art	Clipart	Product	Real	Avg
OpenClip ZS	49.4	24.6	59.0	59.3	48.1
CORAL	33.0	29.4	50.0	58.0	42.6
SAGM	36.8	30.7	51.7	58.7	44.5
ERM	36.0	28.1	51.3	56.0	42.9
LP-FT	37.2	29.7	52.0	54.7	43.4
SWAD	43.9	37.1	56.0	62.7	49.9
MIRO	49.4	39.6	62.7	74.7	56.6
VL2V-SD	56.4	39.3	65.3	65.3	56.6
Attn. Tune	46.0	36.1	59.7	64.0	51.4
Model Parameter Averaging (MPA)	46.0	36.4	55.7	66.0	51.0
CLIPOOD	60.3	44.4	73.3	78.0	63.9
MIRO + SWAD	55.2	44.7	63.3	72.7	59.0
MIRO + MPA	53.5	44.1	65.7	76.7	60.0

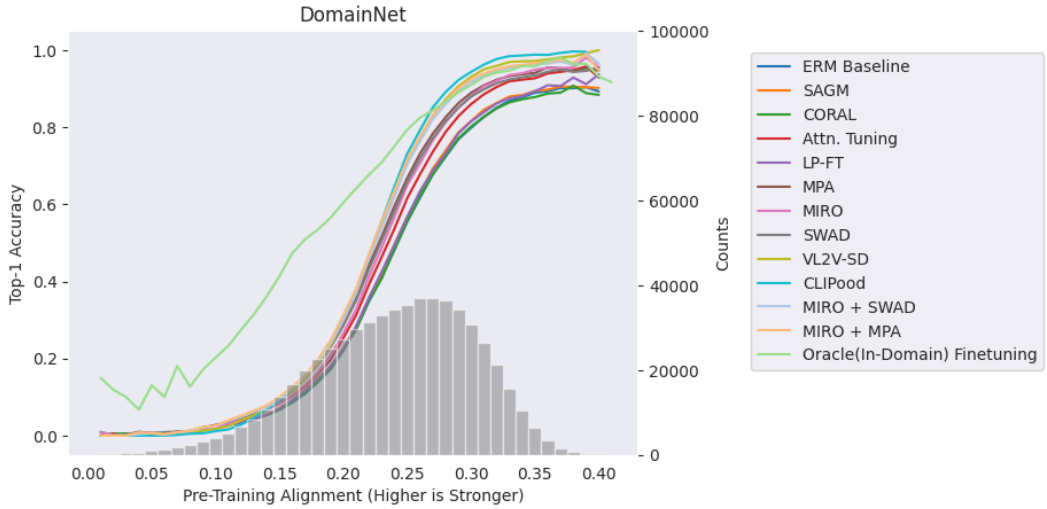

Figure 13: Plotting AlignmentScore vs Top-1 Accuracy on the DomainNet dataset.

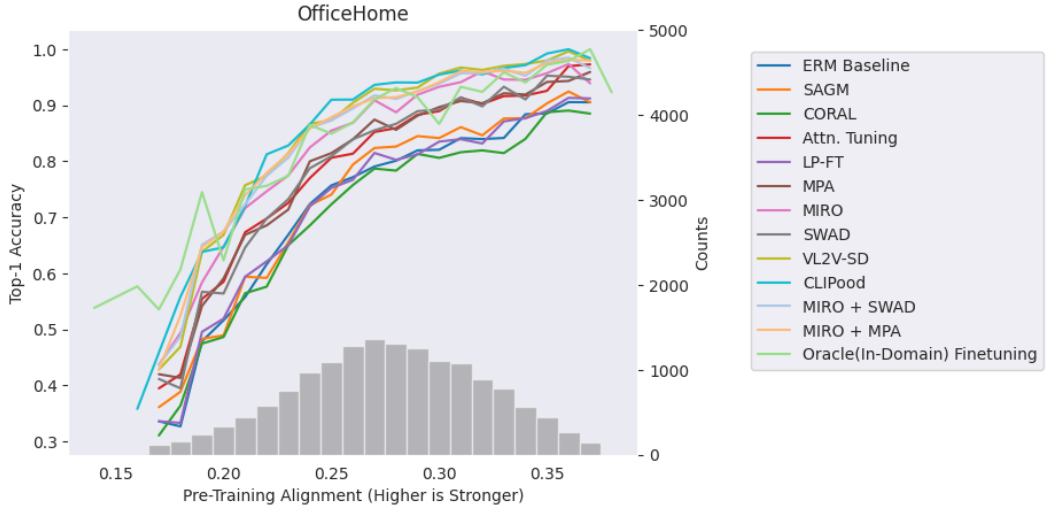

Figure 14: Plotting AlignmentScore vs Top-1 Accuracy on the OfficeHome dataset.

Table 11: Per-domain breakdown for OfficeHome (DomainBed-IP)

Method	Art	Clipart	Product	Real	Avg
OpenClip ZS	88.5	78.0	95.4	93.9	88.9
CORAL	71.6	62.9	85.8	84.0	76.1
SAGM	75.7	70.8	87.0	84.5	79.5
ERM*	74.1	67.4	86.7	84.1	78.1
LP-FT	75.2	66.9	88.9	83.0	78.5
SWAD	81.4	77.8	91.8	88.2	84.8
MIRO	88.3	81.1	93.7	92.1	88.8
VL2V-SD	91.0	83.8	96.7	94.2	91.4
Attn. Tune	86.0	75.1	89.5	88.7	84.8
Model Parameter Averaging (MPA)	83.6	77.1	91.1	88.5	85.1
CLIPOOD (Shu et al., 2023)	92.3	81.3	96.0	94.2	90.9
MIRO + SWAD	90.4	83.2	95.5	92.8	90.5
MIRO + MPA	90.6	83.9	95.4	92.9	90.7

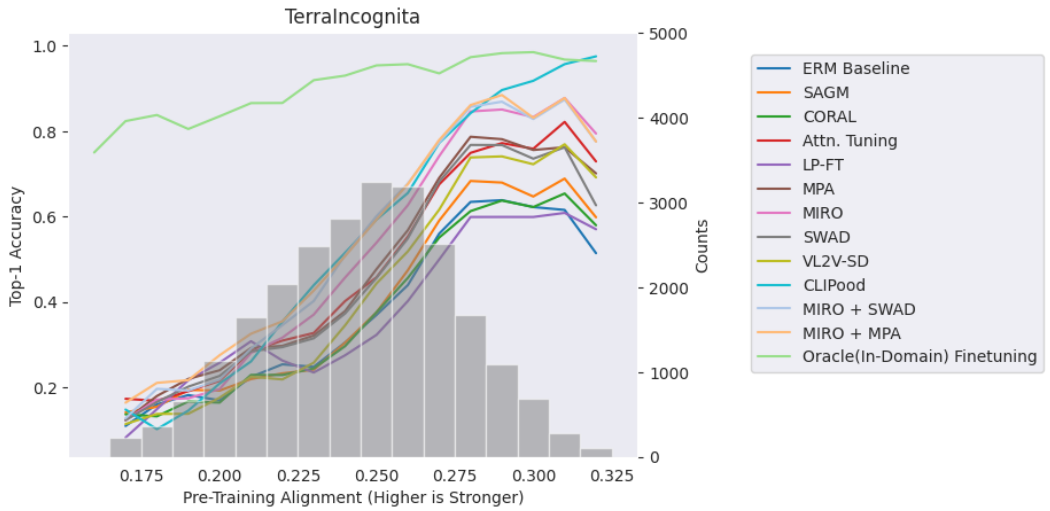

Figure 15: Plotting AlignmentScore vs Top-1 Accuracy on the TerraIncognita dataset.

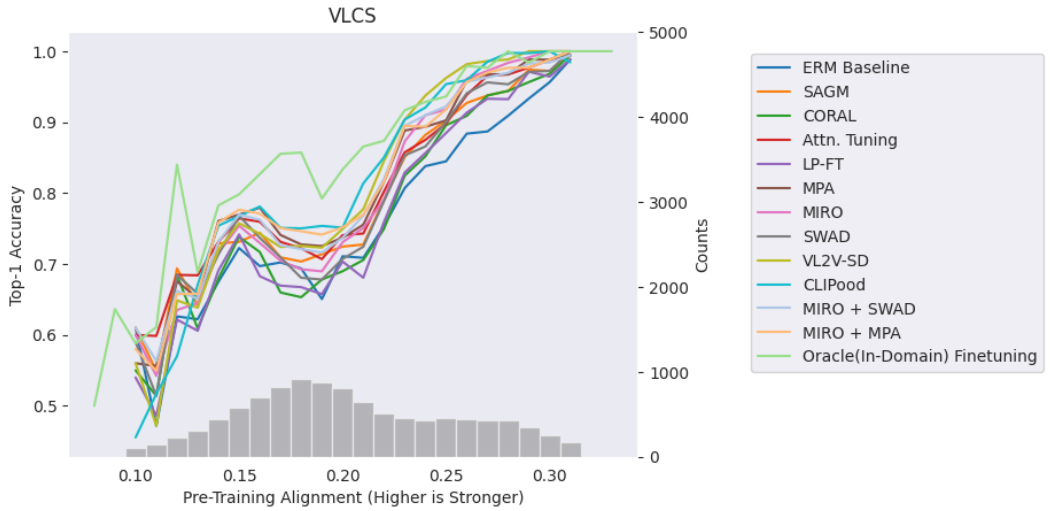

Figure 16: Plotting AlignmentScore vs Top-1 Accuracy on the VLCS dataset.

Table 12: Per-domain breakdown for OfficeHome (DomainBed-All)

Method	Art	Clipart	Product	Real	Avg
OpenClip ZS	83.4	73.2	92.4	92.6	85.4
CORAL	66.6	60.1	83.0	83.0	73.2
SAGM	70.7	67.1	84.3	83.6	76.4
ERM*	69.2	63.9	83.9	83.1	75.0
LP-FT	70.3	63.6	86.0	82.0	75.5
SWAD	76.6	74.3	89.0	87.2	81.8
MIRO	83.2	77.5	91.2	91.4	85.8
VL2V-SD	86.4	79.7	94.1	93.1	88.3
Attn. Tune	80.8	71.7	87.2	87.8	81.9
Model Parameter Averaging (MPA)	78.7	73.4	88.4	87.6	82.0
CLIPOOD	87.9	77.8	94.1	93.6	88.3
MIRO + SWAD	85.6	79.9	93.0	92.1	87.6
MIRO + MPA	85.6	80.5	93.0	92.3	87.9

Table 13: Per-domain breakdown for TerraIncognita (DomainBed-OOP)

Method	L100	L38	L43	L46	Avg
OpenClip ZS	5.1	0.0	6.4	6.6	4.5
CORAL	13.9	8.1	21.1	21.1	16.0
SAGM	17.2	7.8	20.2	32.2	19.3
ERM*	13.1	9.6	22.9	20.5	16.5
LP-FT	16.7	5.1	25.6	44.9	23.1
SWAD	20.7	8.2	26.9	28.2	21.0
MIRO	19.4	6.6	30.0	17.9	18.5
VL2V-SD	9.3	5.6	20.2	28.4	15.9
Attn. Tune	20.5	10.7	24.8	25.3	20.3
Model Parameter Averaging (MPA)	21.7	8.6	30.9	27.6	22.2
CLIPOOD	37.9	11.3	21.6	8.9	19.9
MIRO + SWAD	22.5	5.9	30.3	25.9	21.1
MIRO + MPA	24.8	9.6	32.5	32.8	24.9

Table 14: Per-domain breakdown for TerraIncognita (DomainBed-IP)

Method	L100	L38	L43	L46	Avg
OpenClip ZS	52.3	23.2	36.5	35.1	36.8
CORAL	46.4	35.3	56.9	32.8	42.9
SAGM	55.1	38.7	52.5	29.5	44.0
ERM*	37.4	38.0	55.2	37.5	42.0
LP-FT	50.7	36.5	58.1	18.2	40.9
SWAD	60.1	41.7	65.7	43.5	52.7
MIRO	69.5	50.2	69.7	46.1	58.9
VL2V-SD	52.8	38.4	57.6	43.8	48.1
Attn. Tune	52.4	44.0	68.0	47.5	53.0
Model Parameter Averaging (MPA)	63.8	41.4	67.9	44.7	54.4
CLIPOOD	77.7	56.4	69.0	51.0	63.5
MIRO + SWAD	68.9	54.8	73.4	51.2	62.1
MIRO + MPA	69.4	55.9	73.6	51.4	62.6

Table 15: Per-domain breakdown for TerraIncognita (DomainBed-All)

Method	L100	L38	L43	L46	Avg
OpenClip ZS	48.2	20.9	31.0	32.6	33.2
CORAL	43.6	32.7	50.4	31.8	39.6
SAGM	51.9	35.8	46.6	29.7	41.0
ERM*	35.3	35.3	49.3	36.0	39.0
LP-FT	47.8	33.5	52.1	20.5	38.5
SWAD	56.7	38.5	58.6	42.2	49.0
MIRO	65.2	46.0	62.4	43.7	54.3
VL2V-SD	49.1	35.3	50.8	42.5	44.4
Attn. Tune	49.7	40.8	60.1	45.6	49.1
Model Parameter Averaging (MPA)	60.1	38.3	61.1	43.2	50.7
CLIPOOD	74.3	52.1	60.4	47.4	58.5
MIRO + SWAD	64.9	50.1	65.5	49.0	57.4
MIRO + MPA	65.6	51.5	66.0	49.8	58.2

Table 16: Comparison of Methods for DomainNet Dataset (DomainBed-OOP)

Method	Clp	Inf	Pnt	Qkdr	Real	Skt	Avg
OpenClip ZS	29.2	43.5	28.7	0.0	35.5	21.2	26.3
CORAL	34.9	19.2	26.9	5.7	24.6	22.8	22.3
SAGM	36.4	19.4	25.1	6.1	26.8	24.2	23.0
ERM*	36.2	19.0	23.4	5.4	26.6	23.4	22.3
LP-FT	34.7	20.9	25.2	6.1	25.9	23.2	22.7
SWAD	42.5	28.3	33.4	7.6	30.2	29.5	28.6
MIRO	42.5	37.0	27.9	3.5	33.5	25.8	28.4
VL2V-SD	43.0	43.2	34.8	3.0	37.1	29.5	31.8
Attn. Tune	40.4	29.1	29.2	4.3	31.3	26.6	26.8
Model Parameter Averaging (MPA)	42.3	30.9	34.9	7.4	31.6	30.7	29.6
CLIPOOD	39.2	50.2	39.5	2.1	40.9	31.3	33.9
MIRO + SWAD	46.1	40.4	34.0	4.4	35.2	31.7	32.0
MIRO + MPA	46.2	42.6	36.0	4.4	36.0	33.3	33.1

Table 17: Comparison of Methods for DomainNet Dataset (DomainBed-IP)

Method	Clp	Inf	Pnt	Qkdr	Real	Skt	Avg
OpenClip ZS	84.0	84.1	85.5	23.5	91.4	81.1	74.9
CORAL	80.3	52.3	71.1	33.2	71.7	71.2	63.3
SAGM	81.7	52.8	70.2	34.5	73.4	73.1	64.3
ERM*	80.6	53.4	69.0	31.3	73.0	71.6	63.1
LP-FT	80.0	56.5	70.5	34.0	73.9	71.5	64.4
SWAD	85.5	67.1	80.2	41.3	80.1	79.8	72.3
MIRO	85.4	77.7	79.1	34.6	83.2	74.2	72.4
VL2V-SD	88.3	85.6	84.6	38.0	88.3	84.0	78.1
Attn. Tune	83.5	66.1	77.3	32.6	80.3	75.5	69.2
Model Parameter Averaging (MPA)	85.8	69.7	81.6	41.4	81.4	81.4	73.6
CLIPOOD	86.6	85.4	87.6	38.0	91.0	84.7	78.9
MIRO + SWAD	88.2	81.7	83.9	40.8	85.8	81.9	77.0
MIRO + MPA	88.1	83.7	85.5	41.3	86.5	84.0	78.2

Table 18: Comparison of Methods for DomainNet Dataset (DomainBed-All)

Method	Clp	Inf	Pnt	Qkdr	Real	Skt	Avg
OpenClip ZS	74.9	49.6	68.7	12.7	85.7	66.0	59.5
CORAL	72.7	27.1	58.0	20.1	67.1	58.8	50.6
SAGM	74.1	27.4	56.9	20.9	68.9	60.6	51.5
ERM*	73.1	27.4	55.7	19.0	68.5	59.3	50.5
LP-FT	72.4	29.3	57.1	20.7	69.2	59.2	51.3
SWAD	78.0	36.0	66.1	25.2	75.2	66.7	57.9
MIRO	78.0	42.9	64.0	20.0	78.3	61.7	57.5
VL2V-SD	80.5	47.8	69.5	21.6	83.1	69.8	62.0
Attn. Tune	76.1	36.0	63.0	19.2	75.4	62.9	55.4
Model Parameter Averaging (MPA)	78.3	37.9	67.4	25.2	76.5	68.2	58.9
CLIPOOD	78.4	52.9	72.6	21.2	85.9	70.7	63.6
MIRO + SWAD	80.8	45.6	68.8	23.7	80.7	68.7	61.4
MIRO + MPA	80.7	47.2	70.4	23.9	81.4	70.6	62.4

Table 19: Per-domain breakdown for VLCS (DomainBed-OOP)

Method	Caltech101	LabelMe	SUN09	VOC2007	Avg
OpenClip ZS	100.0	62.0	77.1	81.6	80.2
CORAL	93.3	54.6	72.9	75.3	74.0
SAGM	80.0	58.8	76.5	78.0	73.3
ERM*	100.0	57.1	73.3	75.3	76.4
LP-FT	80.0	55.4	71.8	75.7	70.7
SWAD	100.0	51.2	79.1	77.7	77.0
MIRO	86.7	52.6	82.9	72.7	73.7
VL2V-SD	100.0	55.0	80.4	81.1	79.1
Attn. Tune	86.7	61.0	77.9	79.0	76.1
Model Parameter Averaging (MPA)	100.0	53.6	83.6	80.9	79.5
CLIPOOD	100.0	55.0	84.9	82.8	80.7
MIRO + SWAD	100.0	56.7	84.7	79.9	80.3
MIRO + MPA	100.0	54.6	83.4	77.4	78.9

Table 20: Per-domain breakdown for VLCS (DomainBed-IP)

Method	Caltech101	LabelMe	SUN09	VOC2007	Avg
OpenClip ZS	99.8	91.0	94.8	97.8	95.9
CORAL	98.2	83.5	84.5	79.8	86.5
SAGM	95.9	84.3	86.3	85.5	88.0
ERM*	96.9	83.7	86.1	74.6	85.3
LP-FT	97.1	83.2	82.8	80.7	86.0
SWAD	97.9	82.9	88.4	84.8	88.5
MIRO	98.9	83.3	93.5	88.2	91.0
VL2V-SD	99.5	83.9	91.8	94.6	92.4
Attn. Tune	98.0	84.7	85.7	86.5	88.7
Model Parameter Averaging (MPA)	98.4	83.0	92.6	88.8	90.7
CLIPOOD	98.9	83.6	93.5	94.0	92.5
MIRO + SWAD	97.6	83.4	92.6	90.6	91.1
MIRO + MPA	98.0	83.2	92.9	90.1	91.0

Table 21: Per-domain breakdown for VLCS (DomainBed-All)

Method	Caltech101	LabelMe	SUN09	VOC2007	Avg
OpenClip ZS	99.8	72.7	71.0	86.0	82.4
CORAL	98.2	66.2	72.7	77.0	78.5
SAGM	95.8	68.8	76.2	80.8	80.4
ERM*	96.9	67.8	73.0	73.9	77.9
LP-FT	97.0	66.4	71.4	77.4	78.0
SWAD	98.0	64.5	77.7	80.3	80.1
MIRO	98.7	65.3	81.2	79.3	81.1
VL2V-SD	99.5	66.6	78.8	86.0	82.7
Attn. Tune	97.9	70.3	77.2	81.9	81.8
Model Parameter Averaging (MPA)	98.4	65.7	81.3	83.7	82.3
CLIPOOD	98.9	66.7	81.6	86.6	83.4
MIRO + SWAD	97.6	66.4	81.6	82.6	82.0
MIRO + MPA	98.0	67.4	82.2	83.6	82.8

Table 22: Per-domain breakdown for PACS (DomainBed-OOP)

Method	Art	Cartoon	Photo	Sketch	Avg
OpenClip ZS	96.4	95.9	95.7	37.7	81.4
CORAL	80.4	84.3	89.5	42.2	74.1
SAGM	74.4	78.1	89.5	54.7	74.2
ERM*	75.9	86.8	91.6	53.2	76.9
LP-FT	74.2	85.9	97.9	56.3	78.6
SWAD	84.6	81.6	95.8	54.3	79.1
MIRO	94.2	94.1	97.9	52.8	84.7
VL2V-SD	93.5	96.5	97.9	52.2	85.0
Attn. Tune	94.0	91.4	95.8	55.7	84.2
Model Parameter Averaging (MPA)	94.0	88.9	97.9	50.2	82.7
CLIPOOD	96.0	96.8	97.9	58.3	87.2
MIRO + SWAD	96.0	94.9	100.0	50.7	85.4
MIRO + MPA	95.3	95.4	100.0	60.3	87.8

Table 23: Per-domain breakdown for PACS (DomainBed-IP)

Method	Art	Cartoon	Photo	Sketch	Avg
OpenClip ZS	99.7	99.7	99.9	94.6	98.5
CORAL	83.3	89.8	91.8	72.1	84.3
SAGM	89.7	93.0	94.7	82.9	90.1
ERM*	88.7	93.0	91.5	75.2	87.1
LP-FT	85.3	93.7	97.9	84.2	90.3
SWAD	96.4	93.0	97.8	91.0	94.6
MIRO	99.2	96.7	99.9	94.4	97.6
VL2V-SD	99.6	98.9	99.9	93.6	98.0
Attn. Tune	97.3	97.6	98.9	91.7	96.4
Model Parameter Averaging (MPA)	98.6	95.8	98.2	89.2	95.4
CLIPOOD	99.4	99.3	99.9	92.0	97.7
MIRO + SWAD	99.1	97.9	99.9	93.3	97.6
MIRO + MPA	99.0	98.5	100.0	94.7	98.1

Table 24: Per-domain breakdown for PACS (DomainBed-All)

Method	Art	Cartoon	Photo	Sketch	Avg
OpenClip ZS	97.8	98.7	99.8	91.6	97.0
CORAL	81.4	89.2	91.7	70.5	83.2
SAGM	83.4	90.4	94.6	81.4	87.5
ERM*	83.0	92.1	91.5	74.0	85.2
LP-FT	80.5	92.7	97.9	82.7	88.4
SWAD	91.5	91.2	97.8	89.0	92.4
MIRO	97.1	96.4	99.8	92.2	96.4
VL2V-SD	97.7	98.5	99.9	91.3	96.9
Attn. Tune	96.4	96.5	98.8	89.7	95.4
Model Parameter Averaging (MPA)	97.2	94.8	98.2	87.1	94.3
CLIPOOD	98.2	98.8	99.8	90.2	96.8
MIRO + SWAD	98.0	97.4	99.9	91.0	96.6
MIRO + MPA	97.8	98.0	99.9	92.9	97.2

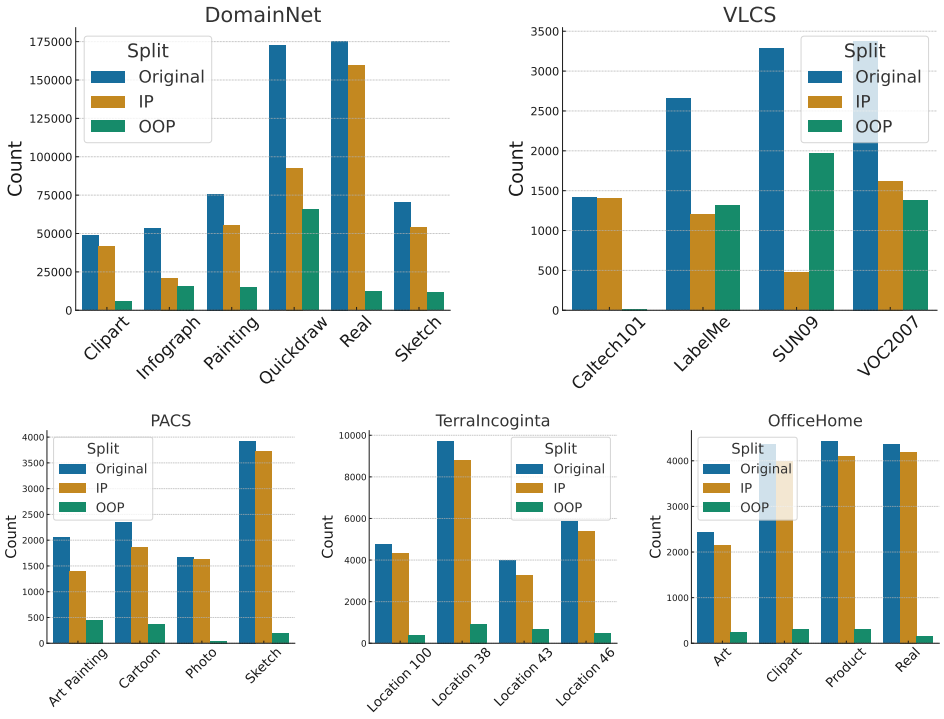

Figure 17: **DomainBed-(IP/OOP) Statistics**: Breakdown of DomainBed-IP and DomainBed-OOP counts, by dataset and domain. Overall, DomainNet and VLCS have the largest fraction of samples falling into DomainBed-OOP.

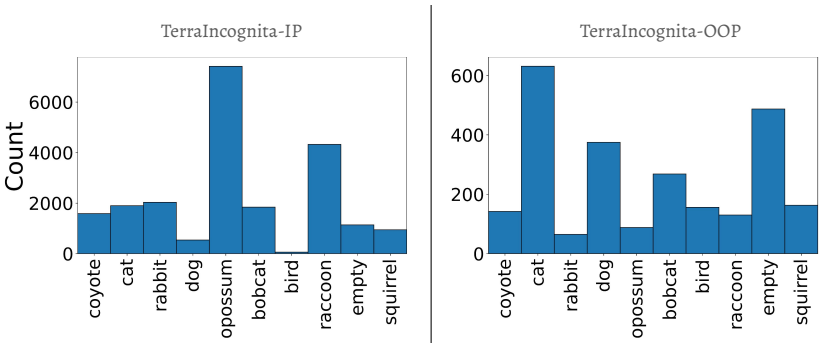

Figure 18: **Class-distribution shift:** TerraIncognita's class distribution differs between DB-IP and DB-OOP, indicating that some classes were better aligned during pretraining.

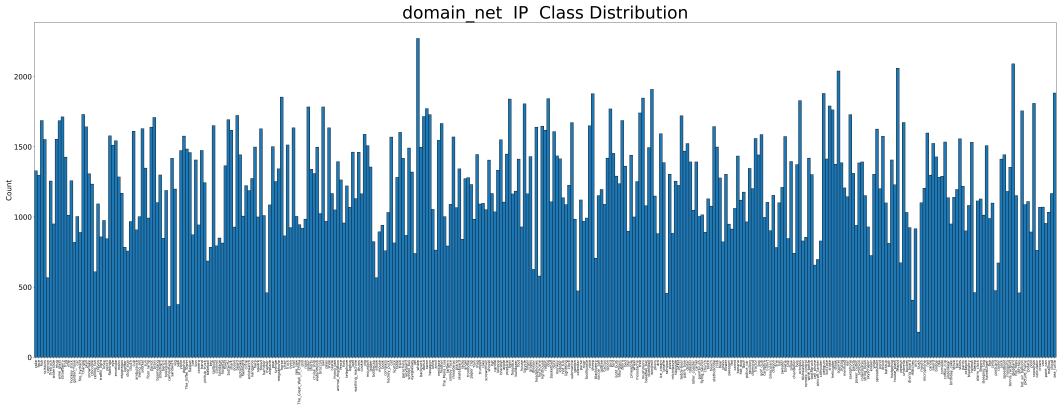

Figure 19: Class distribution of DomainNet-IP. Zoom in on pdf for best viewing.

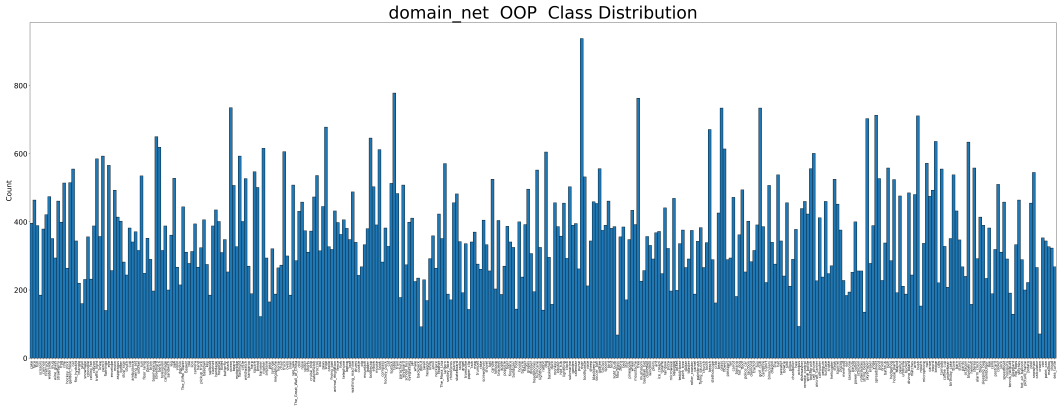

Figure 20: Class distribution of DomainNet-OOP. Zoom in on pdf for best viewing.

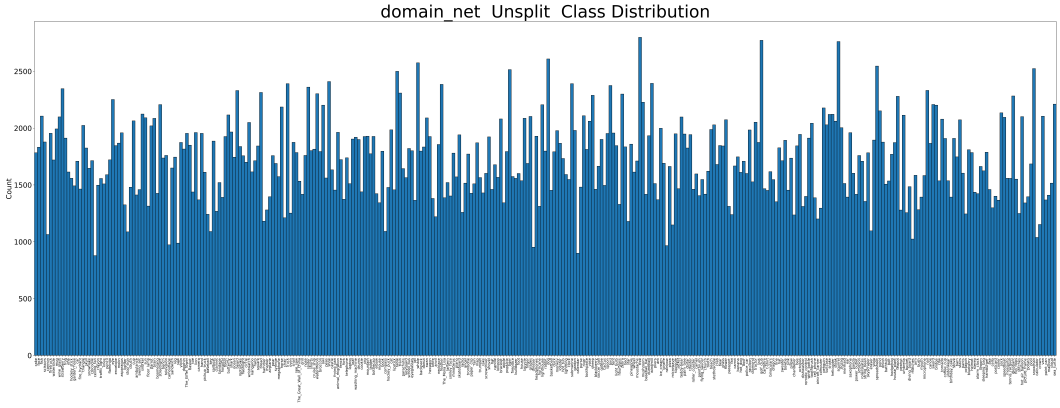

Figure 21: Class distribution of DomainNet before splitting. Zoom in on PDF before viewing.

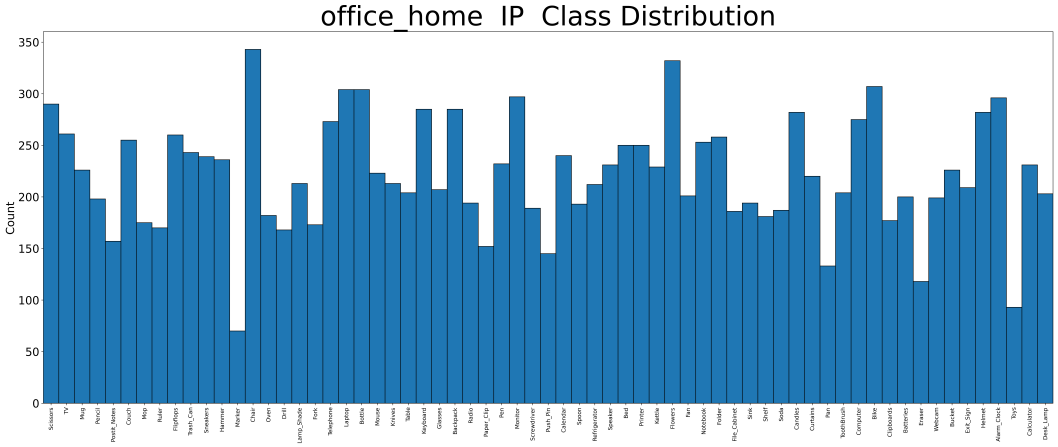

Figure 22: Class distribution of OfficeHome-IP. Zoom in on pdf for best viewing.

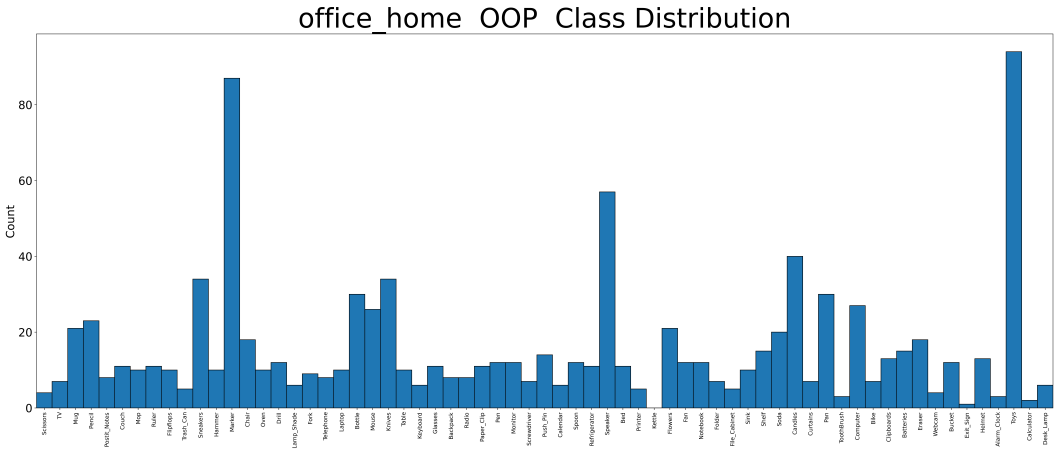

Figure 23: Class distribution of OfficeHome-OOP. Zoom in on pdf for best viewing.

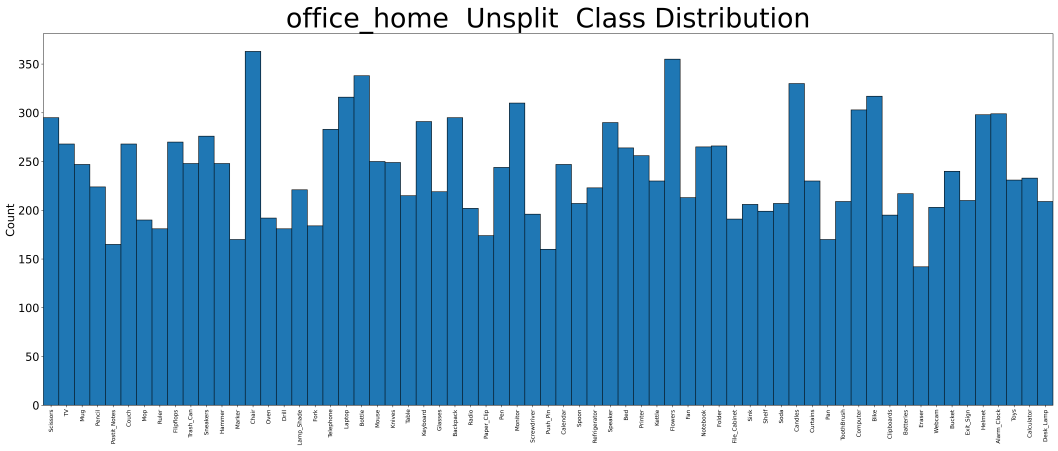

Figure 24: Class distribution of OfficeHome before Splitting. Zoom in on pdf for best viewing.

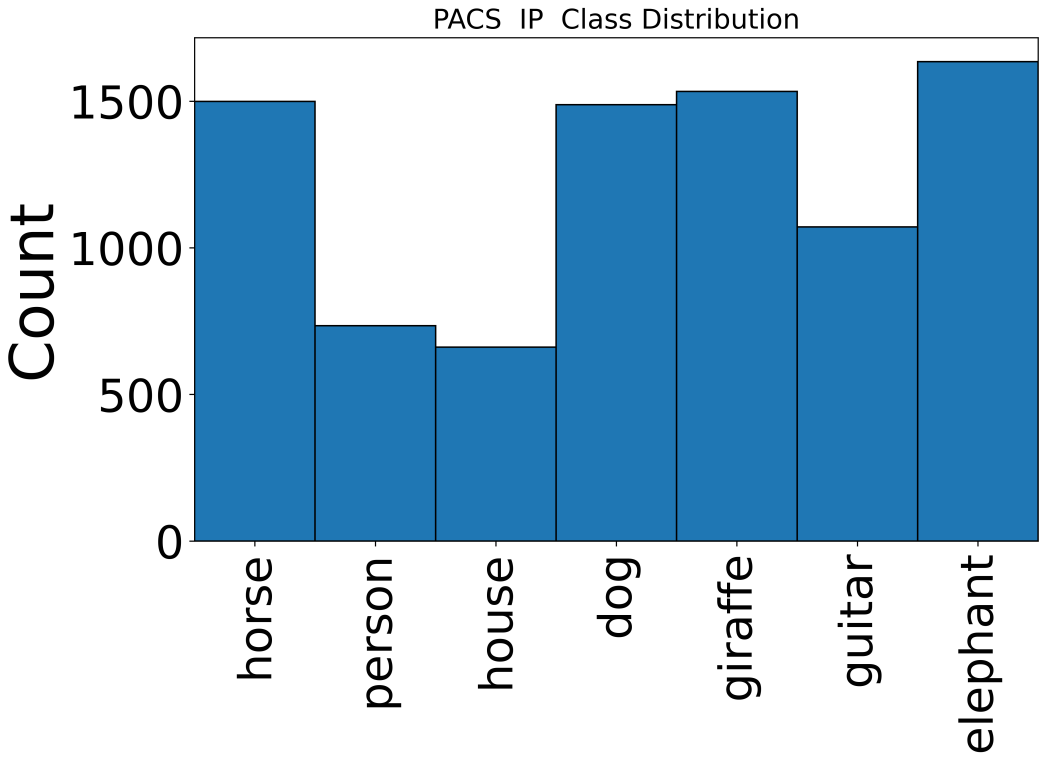

Figure 25: Class distribution of PACS-IP.

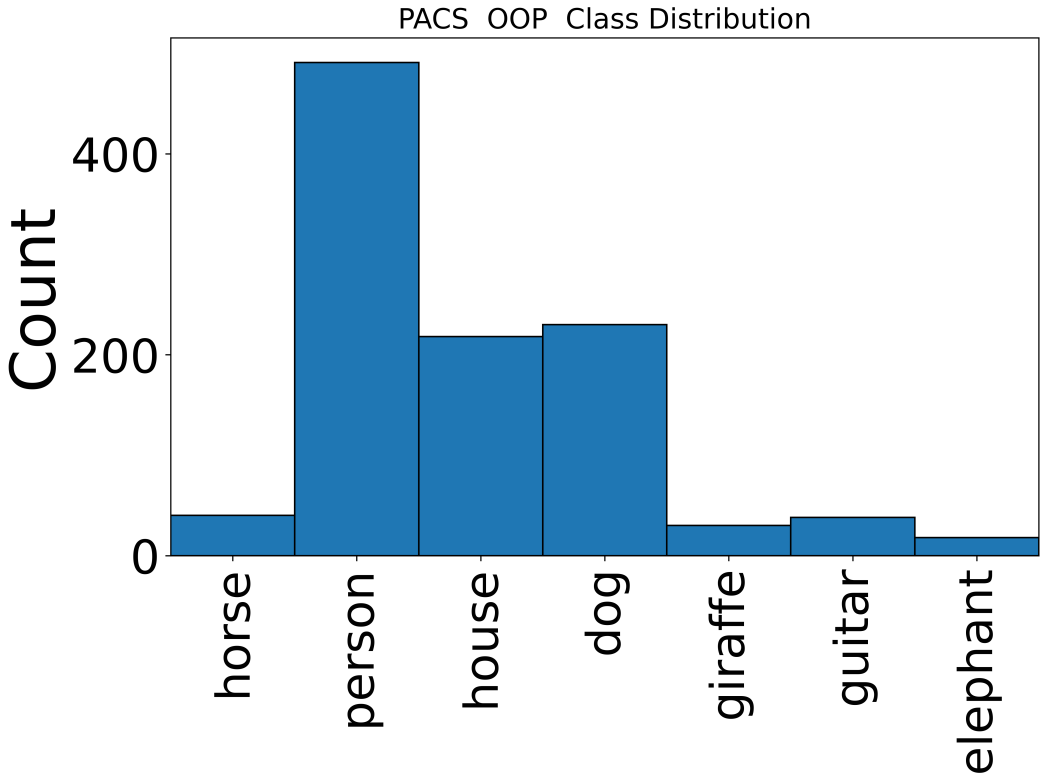

Figure 26: Class distribution of PACS-OOP.

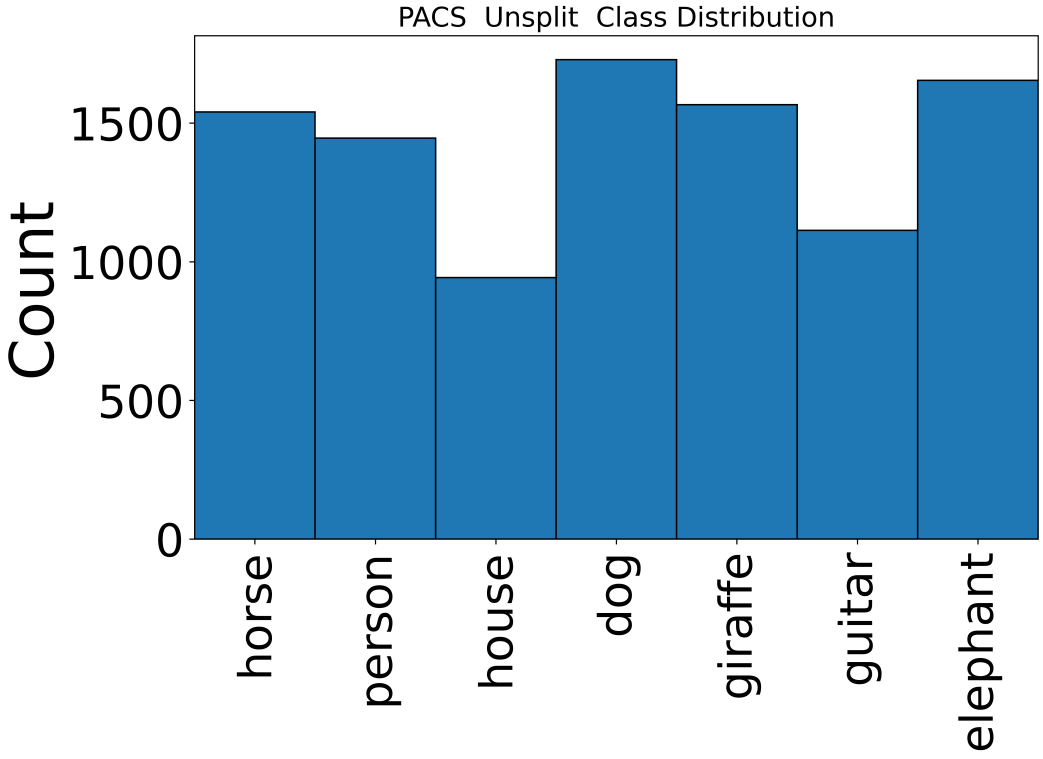

Figure 27: Class distribution of PACS before splitting.

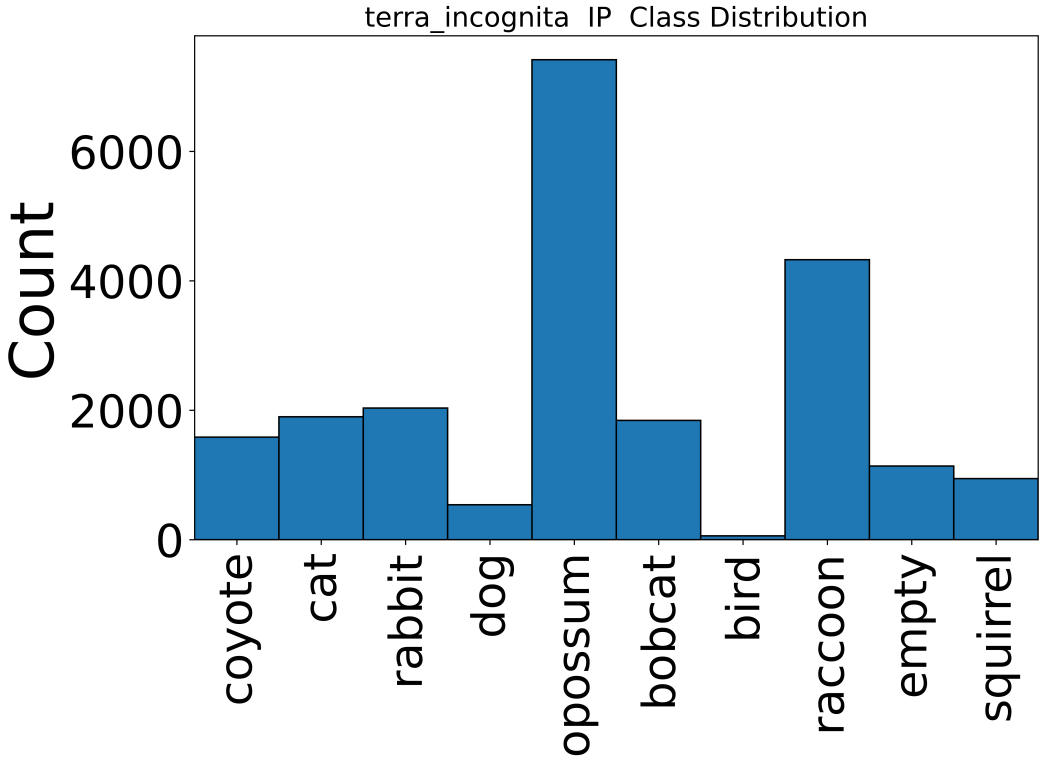

Figure 28: Class distribution of TerraIncognita-IP

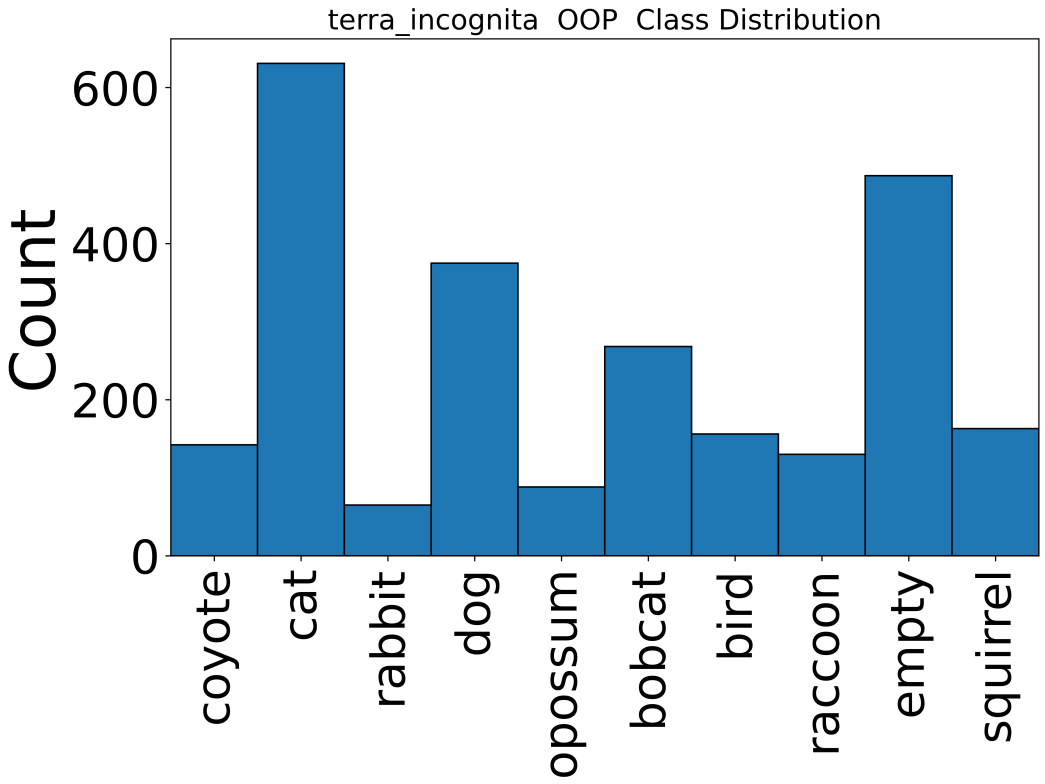

Figure 29: Class distribution of TerraIncognita-OOP

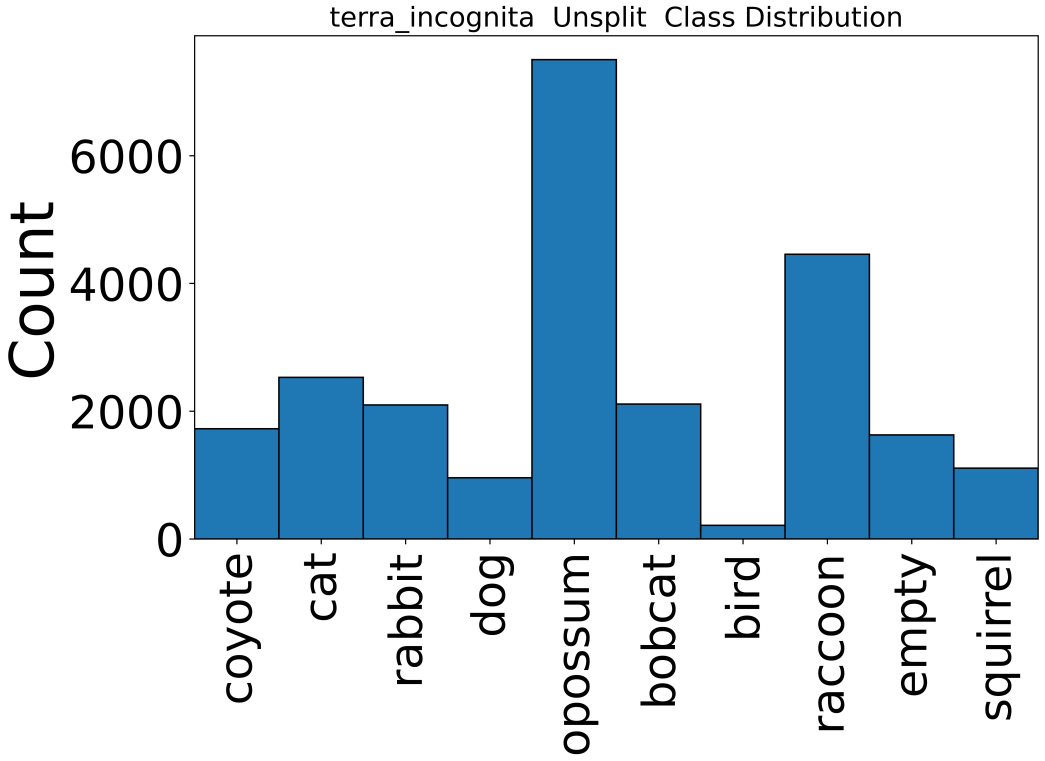

Figure 30: Class distribution of TerraIncognita before splitting.

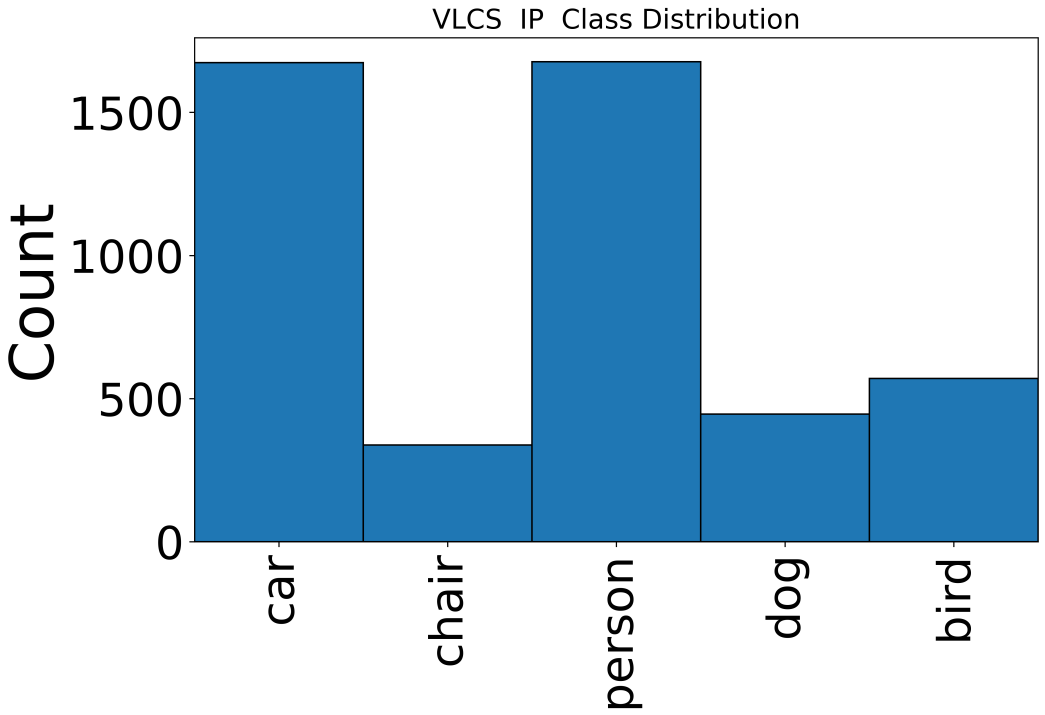

Figure 31: Class distribution of VLCS-IP

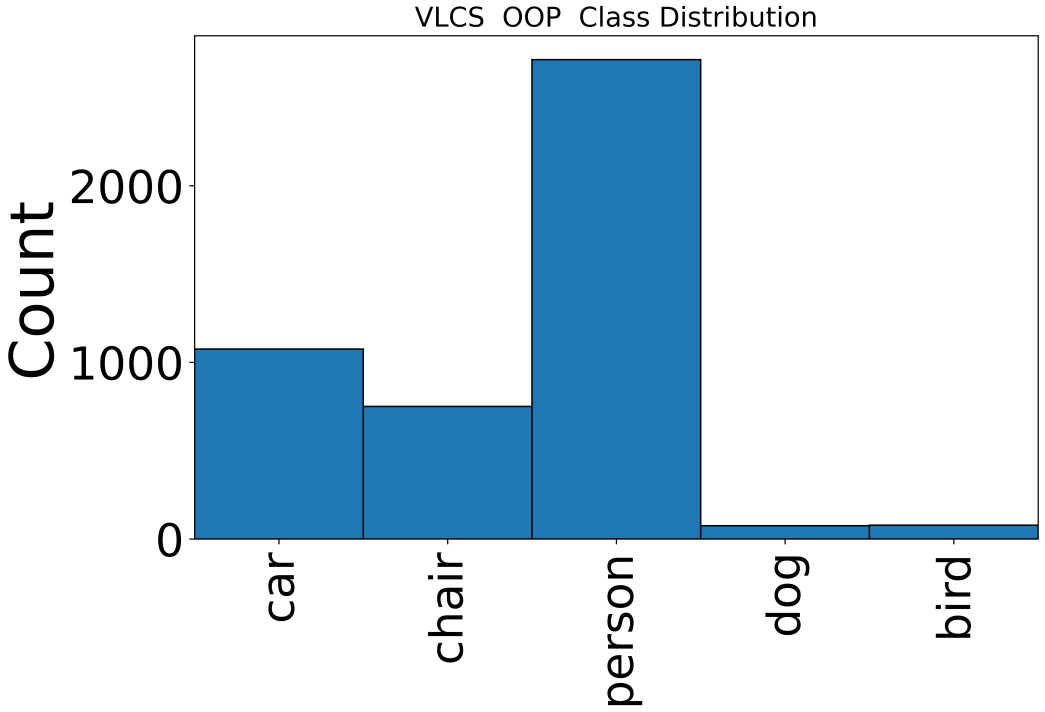

Figure 32: Class distribution of VLCS-OOP

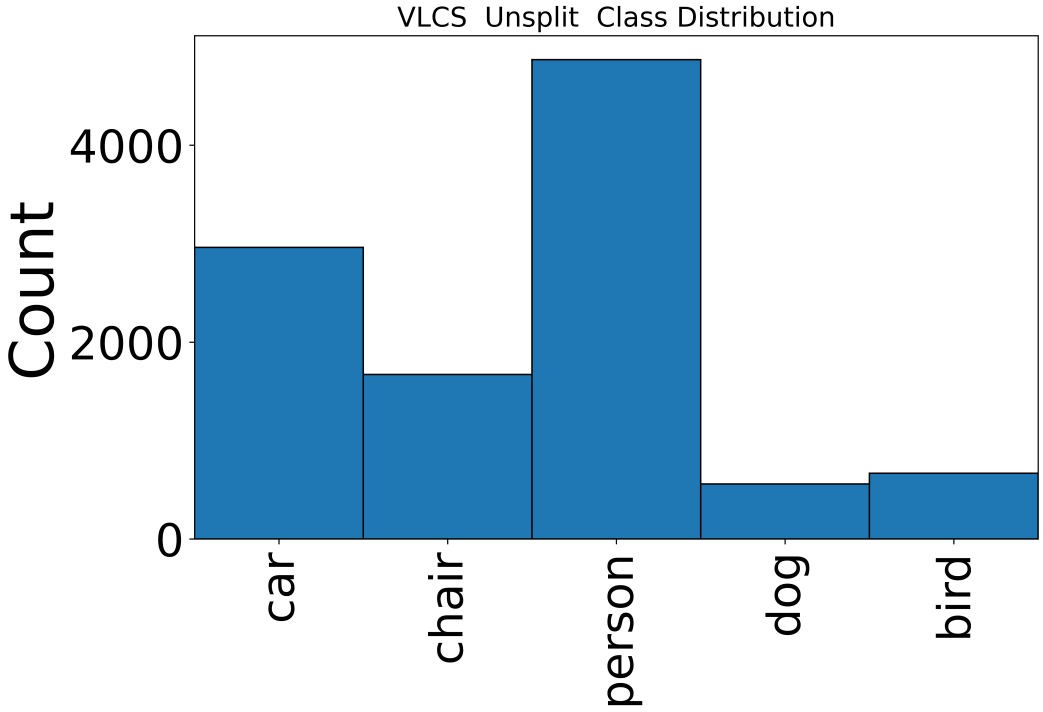

Figure 33: Class distribution of VLCS before splitting.